Applied and
Computational
Mathematics
Division

NISTIR 5557

Computing and Applied Mathematics Laboratory

Lubrication Theory for Reactive Spreading of a Thin Drop

R. J. Braun, B. T. Murray, W. J. Boettinger
and G. B. McFadden

December 1994

Lubrication Theory for Reactive Spreading of a Thin Drop

R. J. Braun
B. T. Murray
W. J. Boettinger
G. B. McFadden

U.S. DEPARTMENT OF COMMERCE
Technology Administration
National Institute of Standards
and Technology
Applied and Computational Mathematics
Division
Computing and Applied Mathematics Laboratory
Gaithersburg, MD 20899

December 1994

Lubrication Theory for Reactive Spreading of a Thin Drop

R.J. Braun,* B.T. Murray, W.J. Boettinger, G.B. McFadden
National Institute of Standards and Technology†
Gaithersburg, MD 20899

January 18, 1995

Abstract

Solder drops spreading on metallic substrates are a reactive form of the wetting problem. A metallic component may diffuse in the liquid toward a metal substrate where it is consumed by a reaction that forms a solid intermetallic phase. The resulting spatial variation in the composition of the drop may cause composition gradients along the free surface of the drop. Together with any thermal gradients along the free surface, Marangoni effects may in turn modify the bulk transport in the spreading drop. Motivated by this situation, we extend lubrication theory for the spreading of thin drops in the presence of gravity and thermocapillarity to include mass transport and solutocapillarity. We use an approximate solute profile in the drop to derive coupled evolution equations for the free surface shape and concentration field. Numerical solutions for the non-reactive (single component) drop agree well with previous theory. In the reactive case, we are only able to compute results for parameters outside of the range for solder materials. Including reactive effects in the model impacts the flow patterns and spreading rates at relatively early times; but by the end of the spreading, solutal effects have died out in the model.

*Corresponding author, Tel.: (301) 975-5913, Fax: (301) 990-4127
†Technology Administration, U.S. Department of Commerce, Washington, D.C.

1. Introduction

The spreading of a droplet on a horizontal surface has been the subject of much research; it is a relatively simple configuration to evaluate the wetting of a surface by a liquid. Such a configuration is also used in the evaluation of wetting in solder (or braze) systems, where a disc of solid solder is melted on a hot substrate, and the subsequent rate and extent of the spreading is measured.[1-5] While there is not a direct correlation between the wettability of the solder and the quality of the joint, good wetting is requisite in the formation of a solder joint of the required geometry. In solder systems (e.g. Pb-Sn or Bi-Sn on Cu or Au), the wetting problem is complicated by a number of effects, including heat and mass transport in the spreading drop, the use of flux to remove non-wetting oxide patches on the substrate, as well as reactions in which intermetallics form at the substrate (e.g., $Cu+Sn \rightarrow Cu_6Sn_5$). The liquid surface tension on the free surface (as well as other properties) depend strongly on the temperature and composition of the molten solder,[6-8] and these variations may in turn affect the fluid dynamics of the spreading through the generation of shear stresses along the free surface, i.e., the Marangoni effect.

In some recent experiments, it was observed that the contact angle in the final shape of the solder drop was in the range of 2 to 16 degrees (see e.g., Ref. 1, 9). At these small angles, the drop's height is much smaller than its radius, and so there is a separation of scales; the lubrication approximation may be applied to the equations of fluid motion to describe the spreading of the thin drop. The presence of the contact line for spreading drops complicates the problem. The physics of the contact line, even without reactions and other processes to complicate matters, is an area of current research. In mathematical models of fluid motion that use the no slip boundary condition, there is a singularity in the shear stress in the fluid at the contact line;[10,11] this singularity may be relieved by allowing some slip of the fluid along the substrate.[12,13] Fortunately for the macroscopic modeling of the fluid flow, only the flow very near the contact line is strongly affected by the form of the slip applied at the substrate[12,14] while the flow far from the contact line is practically indistinguishable for different slip models.

Though the contact angles for the spreading drops in solder experiments[1,2] are small, it appears that the drops only partially wet the substrate. When equilibrium contact angles are zero (perfect wetting), a precursor foot is predicted[15] and found experimentally[16,17] for organics on inert substrates. A precursor foot of this type, with a thickness of hundreds of Angstroms or less, is not observed or predicted for nonzero values of the equilibrium contact angle (partial wetting). In the perfect wetting case, the contact line position is given by a temporal power law; the long time behavior does not obey power law spreading in the partial wetting case.

We believe that the Marangoni effect may play a role in the spreading of solder drops because the transport of heat through the drop sets up tangential temperature gradients along the surface of the drop, which in turn cause surface tension gradients there. These gradients cause shear stresses that either promote or retard spreading. Often the solder drop melts and spreads on a heated substrate, tending to retard spreading for most solder materials. In other situations, however, the solder spreads on a relatively cool substrate while heat is supplied from the surroundings, tending to promote spreading.

Tangential gradients in the alloying element concentration may also cause surface tension gradients. Near the eutectic point for Pb-Sn solder drops, the change in surface tension for a 20K temperature change is roughly equal to a 1wt% concentration change;[6,7] this suggests that the concentration variation may be just as significant as temperature change with regard to the Marangoni

2

effect in the reactive spreading of solder drops. Implicit in this argument is the neglect of the solder flux which is often used in soldering; as a first model, we are ignoring the role of the solder flux in the fluid dynamics of the spreading. Our thought here is to consider Marangoni effects and to evaluate their relative importance during the spreading process. It turns out that the real parameters for solder systems are beyond the reach of the theory and computational method developed here, but we use the solder spreading process as motivation for considering a model of reactive spreading. As much as possible, we base the parameters we use on the Pb-Sn solder system.

The use of lubrication theory for thin drops was first carried out by Greenspan,[18] and has been employed by many workers since. In Greenspan's work,[18,19] an evolution equation for the shape of the free surface of the drop is derived; the speed of the contact line is proportional to the difference between the dynamic contact angle and the advancing equilibrium contact angle. In the limit of small capillary number, that evolution equation is subsequently solved to yield an ordinary differential equation for the contact line position. In a series of papers by Hocking and coworkers,[20–22] the contact angle is assumed constant and matched asymptotic expansions in the limit of small slip coefficient are used to derive an ordinary differential equation for the contact line position. In this approach, the spreading of the drop is limited by viscous dissipation and the slip at the substrate. One discussion of the relationship between these approaches may be found in Ref. 23. Other applications of lubrication theory in spreading include Tanner,[24] de Gennes and coworkers,[15,25] and Brochard-Wyart et al.[26]

We base our model most closely on that developed by Ehrhard and Davis;[27] they suppose that the contact line mobility limits the motion of the drop and they use a modified "Tanner law"[24] as a constitutive relation to determine the motion of the contact line. They extend previous work to include a Marangoni effect due to temperature gradients in the drop. Their theory has been convincingly verified for silicone oil on glass in recent experiments carried out by Ehrhard.[28] The theory has been recently extended by Smith[29] to study drop migration in a horizontal temperature gradient and by Anderson and Davis[30] for volatile droplets on a heated plate. Thermocapillary migration has also been studied by Ford and Nadim.[31]

In this paper, we attempt to study reactive spreading of a drop by modeling the heat and mass transport during the spreading process, and include a simple model for the reaction at the substrate. We generalize the work of Ehrhard and Davis[27] to include gradients in the concentration (of Sn, say, in Pb-Sn drops) caused by the reaction with the substrate (Cu and Cu-Sn alloys in Ref. 1,2). We include this variation by deriving a second evolution equation for the alloying element distribution. In order to derive the second equation, the spatial distribution of the alloying element is assumed to be a polynomial in the vertical coordinate; that is, a Karman-Polhausen type approach is used (see e.g., Ref. 32). This approach was motivated by the study of spin coating with an evaporating solvent carried out by Reisfeld et al.[33,34] The resulting coupled evolution equations for the drop shape and alloy distribution are solved numerically using an implementation of the method of lines; our numerical solution method is similar to that used by Haley and Miksis[35] for a series of drop spreading problems. From these results, and from work in progress,[36] we wish to assess the importance of the solutal Marangoni effect in reactive spreading of drops.

In the next section we formulate the problem; in Section 3, we derive a lubrication theory for the reactive spreading of a planar (two-dimensional) drop on a flat substrate. In Section 4, the numerical methods used to integrate the evolution equations are discussed. Section 5 gives results for reactive and non-reactive spreading drops; discussion and conclusions are given in the final section.

3

2. Formulation

We consider a two-dimensional drop in a Cartesian coordinate system (x', z') on a smooth, horizontal plate in the plane $z' = 0$. The primes denote dimensional variables. The free surface of the drop is given by $z' = h'(x', t')$ and the contact line at $h'(x', t') = 0$ is located at $x' = a'(t')$. The drop is assumed to be symmetric about the line $x' = 0$. The equations governing the velocity, temperature, and concentration fields in the drop are

$$\nabla' \cdot \mathbf{v}' = 0, \tag{2.1}$$

$$\rho \left(\frac{\partial \mathbf{v}'}{\partial t'} + \mathbf{v}' \cdot \nabla' \mathbf{v}' \right) = -\nabla p' + \mu \nabla'^2 \mathbf{v}' - \rho g \mathbf{k}, \tag{2.2}$$

$$\rho c_p \left(\frac{\partial T'}{\partial t'} + \mathbf{v}' \cdot \nabla' T' \right) = \lambda \nabla^2 T', \tag{2.3}$$

$$\frac{\partial c'}{\partial t'} + \mathbf{v}' \cdot \nabla' c' = D \nabla^2 c', \tag{2.4}$$

where $\mathbf{k} = (0, 1)$, $\mathbf{v}' = (u', w')$ is the velocity vector, p' is the pressure, T' is the temperature, and c' is the concentration of Sn in the liquid. Here g is the magnitude of the gravitational acceleration, ρ is the density, μ is the dynamic viscosity, λ is the thermal conductivity of the drop, c_p is the specific heat, and D is the solute diffusivity; all but g are properties of the liquid.

On $z' = 0$ (the substrate), we have

$$w' = 0, \ \beta'(h')u'_{z'} = u', \ \text{and} \ T' = T_w. \tag{2.5}$$

The slip coefficient $\beta'(h')$ may depend on h' and will be specified later. Our Dirichlet condition on the temperature field implies that the substrate is a perfect conductor.

For the concentration boundary condition, we may employ two models for the extraction of Sn from the solder drop as it reacts with the Cu substrate.[2] In the first approach, we could suppose that the boundary behaves like a diffusion couple. In such a model, the concentration at the substrate is fixed for all times greater than the initial time,

$$c' = c_L. \tag{2.6}$$

For example, c_L may be taken as the liquidus concentration from the equilibrium phase diagram at the temperature of the substrate.[2] A more general approach would be to impose a mixed transport condition at the substrate,

$$Dc'_{z'} + H_c(c_L - c') = 0, \tag{2.7}$$

where the coefficient H_c is used to model the reaction rate at the substrate. We have constructed a model using boundary condition (2.7). Equation (2.6) can then be viewed as a limiting case of (2.7) for large H_c. The boundary condition (2.7) is a simple model for the dissolution of the substrate; more complicated models for the reaction there are a subject of current research. We assume that the substrate remains flat and immobile.

On the free surface $z' = h'(x', t')$, we have that

$$w' - \frac{\partial h'}{\partial t'} = \frac{\partial h'}{\partial x'} u', \tag{2.8}$$

$$\mathbf{n} \cdot \nabla c' = 0, \tag{2.9}$$

4

$$n \cdot \mathcal{T}' \cdot n = K'\sigma, \tag{2.10}$$

$$t \cdot \mathcal{T}' \cdot n = t \cdot \nabla'\sigma, \tag{2.11}$$

$$\lambda n \cdot \nabla' T' + \frac{\lambda_{air}}{\delta_{air}}(T' - T_\infty) = 0. \tag{2.12}$$

Here $\mathcal{T}'$ is the stress tensor, n and t are the unit normal and tangent vectors respectively, with n pointing out of the liquid. The heat transfer to passive gas above the drop is modeled by the ratio of the thermal conductivity of the gas λ_{air} and the thermal boundary layer thickness δ_{air}. We also have that the curvature

$$K' = \nabla \cdot \left[\left(1 + |\nabla'h'|^2\right)^{-1/2} \nabla'h' \right]. \tag{2.13}$$

The surface tension σ is given by

$$\sigma(T', c') = \sigma_w - \gamma_T(T' - T_w) - \gamma_c(c' - c_L); \tag{2.14}$$

for solder with the given form for σ, $\gamma_T > 0$ and $\gamma_c < 0$ when considering Sn as the impurity in a Pb-Sn drop.

The initial conditions are

$$h'(x', 0) = h'_0(x'), \ c'(x', h_0, 0) = c'_0(x'), \ h'_0(a_0) = 0, \ a'(0) = a_0. \tag{2.15}$$

At the contact line, initially we have

$$\frac{\partial h'_0}{\partial x'}(a_0) = -\tan\theta_0 \tag{2.16}$$

where θ_0 is the initial contact angle between the free surface of the drop and the substrate. At $x' = 0$, we have the symmetry conditions

$$\frac{\partial h'_0}{\partial x'}(0) = \frac{\partial^3 h'_0}{\partial x'^3}(0) = \frac{\partial c'_0}{\partial x'}(0) = 0. \tag{2.17}$$

The initial volume is given by

$$V_0 = 2 \int_0^{a_0} h'_0(x')dx', \tag{2.18}$$

and will be conserved for all subsequent times. At subsequent times,

$$\frac{\partial h'}{\partial x'}(a'(t'), t') = -\tan\theta(t'), \tag{2.19}$$

$$V_0 = 2 \int_0^{a'(t')} h'(x', t')dx', \tag{2.20}$$

$$\frac{\partial h'}{\partial x'}(0, t') = \frac{\partial^3 h'}{\partial x'^3}(0, t') = \frac{\partial c'}{\partial x'}(0, h', t') = 0. \tag{2.21}$$

The contact line is assumed to move according to the modified "Tanner Law"

$$a'_{t'} = \kappa[\theta(t') - \theta_A]^m; \tag{2.22}$$

5

here $\kappa > 0$ is a constant and θ_A is the advancing equilibrium contact angle for a static contact line. Because we are considering only drops that spread, we need not consider contact angle hysteresis. As pointed out in Ref. 2, the constant κ in the modified Tanner's Law has been estimated to be

$$\kappa = \kappa_0 \frac{\sigma}{\mu} \tag{2.23}$$

where $\kappa_0 = (\pi/4)^3/10 \approx 0.05$ by de Gennes[15] for $m = 3$; see also Ambrose *et al.*[4] for an estimate of $\kappa_0 \approx 0.02$, based also on the work of de Gennes. The magnitude of κ stems from the assumption that the dissipation at the contact line results from the competition of surface tension and viscous forces. A value of $\kappa_0 \approx 0.05$ has been used in the present work based on the estimate given in Ref. 2; hence we have $\kappa = 1.35 \times 10^3 \text{cm/s}$. In general, however, this constant should be determined for each material system;[28] for the case of silicone oil on glass the mobility κ is on the order of 10^{-3}cm/s. We note that the estimate for κ_0 is based on a perfectly wetting system; we have made the assumption that we can use this estimate as an upper bound in the case of partial wetting. We have also made the assumption that θ_A is a constant throughout the spreading process; as pointed out in Ref 2, it need not be true that θ_A be independent of all other variables in the problem. For example, θ_A may decrease during spreading because the action of the solder flux may modify the substrate's surface tension during spreading. Determining such variation and incorporating it into a model of spreading is beyond the scope of this paper. Because of these issues, we choose to deal with only the planar geometry and will seek qualitative comparison with the limited spreading data available to us.

The exponent m for the modified Tanner law is also a subject of ongoing research; a fit of contact angle hysteresis data suggests[27] $m = 3$, while recent research by de Gennes and coworkers suggests a value of $m = 1$.[25] Experimental determinations have found $m = 2.8$ for silicone oil on glass[28] and $m = 2.6$ for silicone oil on a silicon wafer.[37] We shall use $m = 3$ in this work.

3. Lubrication Theory for Reactive Spreading

We next derive appropriate governing equations for the drop taking into account the transport of both solute and heat. The purpose here is to examine the effect of the reaction boundary condition (2.7) on the distribution of solute and the subsequent effect on the spreading of the drop. This model is an extension of the one considered by Ehrhard and Davis.[27] The boundary conditions for the solute are different from the temperature field; the free surface allows no flux of solute, while there is a mixed boundary condition for the concentration on the substrate. For the thermal field, we retain the (mixed) heat transfer condition on the free surface and a fixed temperature on the substrate as in Ref. 27.

We use the following scales:[27]

$$x = \frac{x'}{a_0}, \quad z = \frac{z'}{a_0\theta_0}, \quad t = \frac{\kappa\theta_0^m}{a_0}t'$$

$$u = \frac{u'}{\kappa\theta_0^m}, \quad w = \frac{w'}{\kappa\theta_0^{1+m}}, \quad p = \frac{a_0\theta_0^2}{\mu\kappa\theta_0^m}p'$$

$$T = \frac{T' - T_\infty}{\Delta T}, \quad c = \frac{c' - c_L}{\Delta c}, \quad \Theta = \frac{\theta'}{\theta_0}, \quad V = \frac{V'}{V_0}. \tag{3.1}$$

6

Here $\Delta T = T_w - T_\infty$, $\Delta c = c_m - c_L$ and c_m is the maximum initial concentration in the drop. When these scalings are introduced into the governing equations, we obtain at leading order in the limit $\theta_0 \to 0$,

$$u_x + w_z = 0 \tag{3.2}$$

$$-p_x + u_{zz} = 0, \tag{3.3}$$

$$-p_z - \frac{G}{C} = 0, \tag{3.4}$$

$$T_{zz} = 0 \tag{3.5}$$

$$\theta_0^2 S R \left(c_t + u c_x + w c_z \right) = c_{zz} \tag{3.6}$$

where the subscripts denote partial differentiation, and the dimensionless parameters G, C, R and S will be discussed shortly. For liquid metals, the Schmidt number $S = \mu/\rho D$ is typically large; for example, $S = 81$ for Pb-Sn. We are thus motivated to retain the convective terms in the solute equation in anticipation of the large S balancing θ_0^2 and the Reynolds number $R = \rho \kappa \theta_0^m a_0/\mu$. On $z = 0$, the boundary conditions become

$$u = \frac{\beta_\alpha}{h^\alpha} u_z, \tag{3.7}$$

$$c_z - \mathcal{H}_c c = 0, \tag{3.8}$$

$$w = 0. \tag{3.9}$$

Here we have taken the nondimensional slip coefficient $\beta(h) = \beta_\alpha/h^\alpha$; we shall consider only $\alpha = 1$ in this work. To our knowledge, this form for the slip was first used by Greenspan.[18] On $z = h(x,t)$, we have

$$w - h_t = u h_x, \tag{3.10}$$

$$-Cp = h_{xx}, \tag{3.11}$$

$$u_z = -\frac{1}{\Delta C_c} (c_x + h_x c_z) - \frac{1}{\Delta C} (T_x + h_x T_z), \tag{3.12}$$

$$c_z = 0, \tag{3.13}$$

$$T_z + BT = 0. \tag{3.14}$$

Initially, we have to leading order that

$$h(x,0) = h_0(x),\ h_0(1) = 0,\ a(0) = 1, \tag{3.15}$$

$$\frac{\partial h}{\partial x}(1) = -\frac{3}{2}, \tag{3.16}$$

$$\frac{\partial h_0}{\partial x}(0) = \frac{\partial^3 h_0}{\partial x^3}(0) = 0, \tag{3.17}$$

$$1 = 2 \int_0^1 h_0(x)\,dx, \tag{3.18}$$

$$c = c(x,0); \tag{3.19}$$

for $t > 0$,

$$h(a,t) = 0, \tag{3.20}$$

$$\frac{\partial h}{\partial x}(a, t) = -\Theta(t), \tag{3.21}$$

$$\frac{\partial h}{\partial x}(0, t) = \frac{\partial^3 h}{\partial x^3}(0, t) = \frac{\partial h}{\partial x}(0, h, t) = 0, \tag{3.22}$$

$$1 = 2 \int_0^{a(t)} h(x, t) dx. \tag{3.23}$$

The contact line radius is given by

$$a_t(t) = [\Theta(t) - \Theta_A]^m. \tag{3.24}$$

The nondimensional numbers making an appearance are

$$\mathcal{C} = \frac{\mu \kappa \theta_0^m}{\sigma_w \theta_0^3} \quad (\text{Capillary no.}), \tag{3.25}$$

$$G = \frac{\rho g a_0^2}{\sigma_w} \quad (\text{Bond no.}), \tag{3.26}$$

$$\Delta \mathcal{C} = \frac{\mu \kappa \theta_0^m}{\gamma_T (\Delta T) \theta_0} \quad (\text{Thermocapillary no.}), \tag{3.27}$$

$$\Delta \mathcal{C}_c = \frac{\mu \kappa \theta_0^m}{\gamma_c (\Delta c) \theta_0} \quad (\text{Solutocapillary no.}), \tag{3.28}$$

$$\beta_1 = \frac{\beta_1'}{a_0^2 \theta_0^2} \quad (\text{Slip Coefficient}), \tag{3.29}$$

$$R = \frac{\kappa \theta_0^m a_0}{\mu/\rho} \quad (\text{Reynolds no.}), \tag{3.30}$$

$$S = \frac{\mu/\rho}{D} \quad (\text{Schmidt no.}), \tag{3.31}$$

$$B = \frac{a_0 \theta_0 \lambda_{air}/\delta_{air}}{\lambda} \quad (\text{Biot no.}), \tag{3.32}$$

$$\mathcal{H}_c = \frac{H_c a_0 \theta_0}{D}. \tag{3.33}$$

We expect that the product RS is large and we assume that the Péclet number $\mathcal{P} = \theta_0^2 RS$ is $O(1)$. The nonlinear convective term is then retained in the solute transport equation.

The approximate solution will follow a mix of the approaches of Ehrhard and Davis[27] and Reisfeld et al.;[34] in Ref. 34, a Karman-Polhausen-like approach is used for the concentration field in a large Péclet number limit that is analogous with our case. The idea in our work is that the profile strongly resembles the alloying element profiles for moderate Péclet number transport in drops. This assertion is based on finite element modeling of a drop with a fixed contact line position where we have examined the development of the flow and concentration profiles for various Schmidt numbers.[36] The linear temperature field is determined independent of the flow, but modifies the flow via the tangential stress condition.

We may integrate the solute equation in the bulk in the vertical direction, and using continuity, the kinematic condition on the drop surface, and the flux condition on the substrate, we obtain

$$\frac{\partial}{\partial t} \int_0^h c \, dz + \frac{\partial}{\partial x} \int_0^h uc \, dz = -\frac{c_z(x, 0, t)}{\mathcal{P}}. \tag{3.34}$$

We may integrate the continuity equation in a similar manner to obtain

$$h_t + \frac{\partial}{\partial x} \int_0^h u \, dz = 0. \tag{3.35}$$

Ehrhard and Davis were able to solve the necessary equations in the non-reactive case and derive a single evolution equation for the free surface shape via equation (3.35). In our work, the mass transport equation (3.34) is not easily solved and so we are motivated to find an approximate solution for the solute field in order to reduce the problem to evolution equations for the free surface shape and the appropriate concentration variable. To this point the evolution equations (3.34) and (3.35) are independent of the model used for the reaction at the substrate.

In a manner similar to Ref. 34, we pose the following behavior for the solute field:

$$c = c_2(x, t) + \mathcal{H}_c c_2(x, t) z + c_{\alpha_c}(x, t) z^{\alpha_c}, \tag{3.36}$$

where $\alpha_c > 1$ is a constant; this form is consistent with the flux condition (3.8) on the substrate. In order to satisfy $c_z(x, h, t) = 0$, we eliminate c_{α_c} to obtain

$$c = c_2 + \mathcal{H}_c c_2 \left[z - \frac{h^{1-\alpha_c}}{\alpha_c} z^{\alpha_c} \right]. \tag{3.37}$$

Here $c_2(x, t)$ is the deviation of the concentration from the liquidus on the substrate, and the flux on the substrate is proportional to c_2. This profile resembles those seen in full Navier-Stokes computations for a drop with a stationary contact line, a moderate contact angle, and a moderate Péclet number;[36] this profile may be a poor approximation for the the extremely large Péclet numbers which occur in an actual solder drop. It corresponds more closely to a material with larger diffusivity than those of typical liquid metals. Allowing more complicated spatial dependence in the Karman-Polhausen profile is possible at the expense of adding more free parameters; we choose not to do this.

The z-component of the momentum equation (3.4) can again be used to find the pressure; after using the normal stress boundary condition (3.11), one finds that

$$p(x, z, t) = \frac{G}{C}(h - z) - \frac{1}{C} h_{xx}. \tag{3.38}$$

The x-component of the momentum equation (3.3) can then be used, along with the boundary conditions to find that

$$u(x, z, t) = -\frac{1}{C}(D_{3x}h)\frac{z^2}{2} + A_2\left(z + \frac{\beta_1}{h}\right), \tag{3.39}$$

where

$$A_2 = \frac{1}{C}\left\{ hD_{3x}h + M\frac{h_x}{(1 + Bh)^2} - M_c\left[c_{2x} + \left(1 - \frac{1}{\alpha_c}\right)\mathcal{H}_c\,(c_2 h)_x \right] \right\}, \tag{3.40}$$

and

$$D_{3x}h \equiv (h_{xx} - Gh)_x. \tag{3.41}$$

We have defined the thermal and solutal Marangoni numbers

$$M = \frac{BC}{\Delta C}, \quad \text{and} \quad M_c = \frac{C}{\Delta C_c}. \tag{3.42}$$

9

We may integrate u once more in the vertical direction; we find that

$$\tilde{u} = \int_0^h u \, dz = -\frac{1}{C}(D_{3x}h)\frac{h^3}{6} + A_2\left(\frac{h^2}{2} + \beta_1\right). \tag{3.43}$$

Substitution into Eq. (3.35), $h_t + \tilde{u}_x = 0$, gives an evolution equation for the shape of the free surface of the drop:

$$h_t + \frac{1}{C}\left\{\left(\frac{h^3}{3} + \beta_1 h\right)D_{3x}h + \right.$$
$$\left.\left(\frac{h^2}{2} + \beta_1\right)\left(\frac{Mh_x}{(1+Bh)^2} - M_c\left[c_{2x} + \left(1 - \frac{1}{\alpha_c}\right)\mathcal{H}_c(c_2h)_x\right]\right)\right\}_x = 0. \tag{3.44}$$

We may then evaluate the integrals required in Eq. (3.34); the result is a second evolution equation, viz.

$$\left[c_2h + \mathcal{H}_c b_1 c_2 h^2\right]_t + \left[c_2\tilde{u} + \mathcal{H}_c c_2 A_4\right]_x = -\frac{\mathcal{H}_c}{\mathcal{P}}c_2, \tag{3.45}$$

where

$$A_4 = f_1 + A_2 f_2, \tag{3.46}$$

$$f_1 = -\frac{1}{2C}b_3 h^4 D_{3x}h, \quad f_2 = b_2 h^3 + b_1 \beta_1 h, \tag{3.47}$$

and

$$b_k = \frac{\alpha_c(\alpha_c + k) - (k+1)}{\alpha_c(\alpha_c + k)(k+1)}, \quad k = 1, 2, 3. \tag{3.48}$$

The evolution equations (3.44) and (3.45) with attendant boundary conditions constitute our model for reactive spreading; the equations in the limit of infinitely large $\mathcal{H}_c$ may be considered a second model in which the Dirichlet condition on the solute field is $c = 0$. Such a model would consider the reaction at the substrate to be classical interdiffusion with infinitely fast kinetics. We have also carried out computations on this type of model; those results are not reported here.

3.1 Boundary and initial conditions

The evolution equations are also coupled to the contact line motion via

$$a_t = [-h_x(a, t) - \Theta_A]^m. \tag{3.49}$$

Both h and c_2 are subject to the symmetry conditions at the origin, namely

$$h_x = h_{xxx} = c_{2x} = 0. \tag{3.50}$$

The fluid volume is also conserved,

$$\frac{1}{2} = \int_0^{a(t)} h(x, t) \, dx. \tag{3.51}$$

This is an approximation in our model, since there is some solute leaving the drop, but we assume that the volume of the drop is not affected by this. For the initial condition, we have used

$$c_2(x, 0) = \epsilon h_0^2(x), \tag{3.52}$$

where the amplitude ϵ is chosen such that $c(0, h, 0) = 1$. The above expression for the initial solute profile must satisfy $c_{2x}(x = a) = 0$; this boundary condition, in addition to $c_2 = 0$ are seen to be natural for this kind of problem after consideration of the appropriate wedge flow problems;[40,41] in essence we have matched the outer solution we are finding onto the inner wedge flow problem. We thus require the outer solution we find in our evolution equation to have the correct behavior near the contact line.

The initial drop shape for all results presented in this work is given by

$$h_0(x) = \frac{3}{4}(1 - x^2). \tag{3.53}$$

We have adopted this initial condition for the purposes of comparison; however, because we have retained the time derivative in the evolution equations, we could have used any reasonable drop shape. In the limit of small capillary number, the initial distortions from a circular cap will be eliminated relatively quickly compared to the time scale of the spreading.

At this point we would like to emphasize that these initial conditions are in a sense the starting point for a long-time solution to the spreading problem. We are applying this kind of theory for reactive spreading with the thought that the initial transients involving melting are completed and fluid dynamic spreading of a roughly circular cap is beginning.

4. Numerical Integration of the Evolution Equations

The above equations were mapped onto a fixed domain $-1 \leq \xi \leq 1$ by defining $\xi = x/a(t)$; we then have

$$\frac{\partial h(x, t)}{\partial x} \rightarrow \frac{1}{a} \frac{\partial h(\xi, t)}{\partial \xi} \tag{4.1}$$

and

$$\frac{\partial h(x, t)}{\partial t} \rightarrow \left(\frac{\partial}{\partial t} - \frac{a_t \xi}{a} \frac{\partial}{\partial \xi} \right) h(\xi, t). \tag{4.2}$$

The resulting equations are then discretized pseudospectrally using Chebyshev polynomials and collocated at the Gauss-Lobatto points.[38] An advantage of this approach is that we are able to work in the physical domain and use a differentiation matrix to evaluate the derivatives at the collocation points while obtaining high order accuracy in the discretization. This results in a system of ODEs in time for the elevations of the drop surface at the collocation points and the radius of the drop, as well as the algebraic condition which conserves volume. Due to the symmetry of the drop, we need only solve the equations on $0 < \xi < 1$. This system of differential-algebraic equations (DAEs) is then solved by the package DASSL,[39] which uses an adaptive, implicit time stepping scheme that is up to 5th-order accurate. Our solution to the DAE's is a more accurate approach than the first order scheme (in time) used by Haley and Miksis;[35] otherwise the approaches are practically identical.

11

5. Results

The parameters for Pb-Sn solder near the eutectic point as well as initial data used in the calculations are given in Table 1. We point out that these parameters are what we would like to use for computation for solder drops. We are able to achieve the desired parameters for a non-reactive drop in Section 5.1; for the reactive case we discuss what we can achieve in Section 5.2.

5.1 Non-reactive Spreading

For this case, the drop is at uniform concentration. The evolution equations reduce to a single evolution equation for the free surface shape; that equation is a modified version of Ehrhard and Davis' result, *viz.*,

$$h_t + \frac{1}{C}\left[\left(\frac{h^3}{3} + \beta_1 h\right)(h_{xx} - Gh)_x + M\frac{(h^2/2 + \beta_1)\,h_x}{(1 + Bh)^2}\right]_x = 0. \tag{5.1}$$

The modification to their model is that we solve the evolution equation while retaining the time derivative and a nonzero Biot number in the denominator of the Marangoni term. This equation is subject to the symmetry conditions at the origin, the contact line constitutive law, and conservation of volume.

In Figure 1, we show results for the pure capillary case $G = M = 0$; numerical results using the technique described above are shown for two different advancing equilibrium contact angles, $\Theta_A = 0.1$ and $\Theta_A = 0$; Figure 2 shows the (approximate) slope δ of the $\ln a$ *vs.* $\ln t$ plot. Since for $\delta =$ constant the growth of the radius is proportional to t^δ, we refer to δ as the spreading exponent. The chain-dashed curve shown in these figures is the solution to the $C = 0$ problem.[15,18,27] In the planar geometry, for $C = 0$ we must solve an ODE for the contact line radius

$$a_t = \left(\frac{3}{2a^2} - \Theta_A\right), \ a(0) = 1. \tag{5.2}$$

The steady-state contact line radius is given by $a_\infty = \sqrt{3/(2\Theta_A)}$. Good agreement at long times is obtained with the numerical method; it is expected that the two should agree at long times since the freedom to specify an arbitrary initial shape for the drop shape is given up when $C = 0$ in the problem. The final radius is attained very accurately. We also note that the radius of the drop increases in proportion to t^δ, $\delta = 1/7$ for $\Theta_A = 0$ in Figure 2, as is expected for the planar geometry and capillary spreading.[24,27] We view this case as a verification of the numerical method, especially for the long times required in the computation. It is clear that $t^{1/7}$ spreading is not obtained for nonzero advancing equilibrium contact angles.

We also note that in some work,[4,5] the $C = \Theta_A = 0$ (perfect wetting) solution has been applied to the spreading of solder droplets where $\Theta_A \neq 0$ (partial wetting). It is clear why the discrepancy in time scale between the experiments and the theory exists in light of the difference exhibited in Figures 1 and 2.

The effect of gravity is included in results shown in Figures 3 and 4. In these figures, cases for $\Theta_A = 0$ and $\Theta_A = 0.1$ are shown as well as a quasistatic case $C = 0$, $\Theta_A = 0.1$. The simplified problem that is solved for $C = 0$ is given by (after Ref. 27)

$$a_t = \left[-\frac{G}{2(1 - aG^{1/2}\coth aG^{1/2})} - \Theta_A\right]^m, \ a(0) = 1. \tag{5.3}$$

12

Long time agreement is again observed between the numerics and the quasistatic solutions of Ref. 27. The $C = 0$ solution spreads faster at early times, and then the two become indistinguishable at late times; see also Table 2. At long times, we recover $t^{1/4}$ spreading in the $\Theta_A = 0$ case; this gravity-dominated regime occurs after an early transient which resembles pure capillary spreading ($t^{1/7}$). This behavior is what is expected based on previous experimental and theoretical work.[24,27] Once again, power-law spreading is not achieved for $\Theta_A \neq 0$.

Thermal Marangoni effects are included in the results shown in Figures 5 and 6; here we have neglected the effect of gravity. In these figures, the thermal Marangoni effect retards spreading, as would be expected in solder drops that are heated from below. We find that the final radius agrees well with the asymptotic result given in Ref. 27 for $M \ll 1$ as given in Table 3. The data for Table 3 is for $\Theta_A = 0.5$. The magnitude of the Marangoni effect given by $M = 0.01$ is expected to be the maximum which could be reasonably expected in a solder drop under the conditions of the experiments in Refs. 1, 2 and is based on the data in Refs. 6, 7. For $\Theta_A = 0.1$, the computed final radius is reduced by about 10% from the $M = 0$ case; this is a much bigger effect than for the larger Θ_A data in the table.

As is shown in Figure 6, there is no longer true power-law spreading for $\Theta_A \neq 0$, but there is a period at early times, where a roughly constant δ exists. A rapid decrease in the rate of spreading occurs at later times, and our numerical solution suggests that spreading stops even for $\Theta_A = 0$ as predicted by Ref. 27. Our numerics break down before the final radius is reached however, due to the development of singularities in the higher derivatives, as pointed out in Ref. 27. In order to accurately represent the approach to the final radius without enforcing a quasistatic behavior would require more sophisticated numerical methods than we have employed here.

Figure 7 shows radius $vs.$ time results when gravity and thermocapillarity are included. When the Marangoni number is positive (negative), the temperature field corresponds to a hotter (colder) substrate than the surroundings; this situation retards (promotes) spreading compared to the $M = 0$ case when gravity is included. For the parameters used here, the case when Marangoni flow retards spreading with $G = 0.15$ is very close to the case $M = G = 0$ shown in Figure 1.

In Figure 8, we display results that show the sensitivity of the model to the slip parameter β_1 when the Marangoni effect is included. Greenspan[18] showed that when the capillary number is small, the solutions for the spreading drop are insensitive to the slip parameter; in the absence of Marangoni effects, our numerics bear this out. When Marangoni effects are included however, we must have a small slip parameter in order to achieve the correct final radius.

In Figure 9, we show the shape of the free surface of the drop including gravity and thermocapillarity for an advancing contact angle $\Theta_A = 0$. The drops are thin in physical coordinates, but do not necessarily appear thin in the scaled coordinates. At late times, an inflection point appears near the outside edge of the drop; in this case, the radius at the end of the computation is almost 7.5. The case shown for $\Theta_A = 0$ displays this inflection most clearly. For nonzero Θ_A, the inflection point is difficult to detect visually.

5.2 Reactive Spreading

Figures 10 and 11 show results from the numerical solution of the evolution equations (3.44) and (3.45); here, $\mathcal{P} = 200$, $\mathcal{H}_c = 2000$, $C = .05$, $\Theta_A = 0.1$, $G = 0$ and $M = -M_c = 0.01$ which we designate case I. We may think of the spreading as taking place between the angles of 45° and 3°; then $t = 6600$ is roughly one second. This choice of Θ_A implies a 15 times reduction in the slope of

13

the drop surface at the contact line during spreading. We have computed solutions in this section for drops whose volume has initial radius $a_0 = 0.17$cm at $\theta_0 = 45°$. The Marangoni numbers were fixed at there values based on the estimates in Table 1, with the expectation that the two effects are of comparable magnitude.

We see in Figure 10 that at early times the solutal Marangoni effect retards spreading since the radius at each instant of time lags that of the corresponding conditions for the non-reactive drop with or without the thermal Marangoni effect. This slowing of the spreading relative to non-reactive cases disappears relatively quickly; the excess solute in the drop has been extracted by the substrate and the slowing of the contact line abates. The absence of solute (i.e., the arrival of c' at c_L) then eliminates the solutal Marangoni effect.

In Figure 11, the concentration of solute at the top of the drop and the normalized total amount of solute are shown as a function of time. It is clear that the drop has an increased concentration at the top of the drop when compared to the initial state for some times. The total amount of solute in half of the drop $I_c(t)$ decays monotonically, as shown by the lower curve, where

$$I_c(t) = \int_0^a \int_0^h c(x, z, t) \, dx \, dz \tag{5.4}$$

The increase in the concentration at the top of the drop is an artifact of the model, since diffusion would not allow such an increase; however, since the increase is not large, we are willing to accept such behavior under our stated philosophy of giving Marangoni effects the most favorable circumstances to impact spreading. It is perhaps not surprising that such behavior is possible in our model because we are not solving the mass transport equation pointwise, but we are really satisfying it in an integrated sense by using a Karman-Polhausen profile for the solute field. The increase in local concentration does not appear in problems where there is a fixed concentration on the moving boundary as in Reisfeld et al.,[33,34]

For completeness we show the spreading exponent behavior in Figure 12. Initially, the spreading is slowed and δ is reduced, but it increases later in the spreading while the spreading catches up to the thermal case. At early times, spreading is retarded by the presence of the solute field, and late in the spreading the thermal field retards the spreading.

The behavior of the solute field and stream function are shown in detail in the sequence depicted in Figures 13 through 17. The top (bottom) part of the figure shows the concentration field (stream function). By a fairly early time, the solute concentration has become very small (below the error tolerance of the time integration) and by that time the solutal Marangoni effect plays no further role. In the time that it is operating however, it generates a vortex which retards the spreading in comparison with the case with no Marangoni effects (cf. Figure 12). It is important to note that the maximum of the stream function is near 10^{-1} initially and is about 10^{-5} at the latest time of the calculation. This wide variation in the strength of the flow and the fact that the third derivative of the free surface shape is required to compute the stream function makes this computation an extreme test for the collocation method we have used. Some error due to aliasing is visible in the streamlines at the latest times; the numerical error is compounded by interpolation of the solution from the Chebyshev points (32 or 48 on the half interval) to a fine uniform mesh for contour plotting (200 points). The time scale for the exit of the solute from the drop is set by the Péclet number $\mathcal{P}$ and to a lesser extent by $\mathcal{H}_c$; the time scale of the spreading flow is set primarily by κ, m, and Θ_A. We have used the largest $\mathcal{P}$ for which we could compute solutions. Based on the diffusivity in Table 1, a Péclet number of $\mathcal{P} = 10^4$ to 10^6 would occur in the actual drop. For values of $\mathcal{P} \le 100$,

14

a vortex due to the solutal Marangoni effect did not form.

In carrying out the lubrication approximation, an approximate no-flux boundary condition was applied at the free surface, namely $c_z(x, h, t) = 0$. Mass flux through the free surface of the drop, given by

$$\int_0^a \theta_0 c_x(x, h, t) h_x(x, t) dx,\qquad(5.5)$$

compared to that through the base,

$$\int_0^a c_z(x, 0, t) dx,\qquad(5.6)$$

is at most about $0.3\theta_0$ at $t = 0$, and rapidly decreases to less than $0.05\theta_0$. Clearly the approximation of the no flux boundary condition improves as the initial contact angle θ_0 decreases.

An example of spreading with less extreme deformation of the drop which includes gravity and Marangoni effects is shown in Figures 18 through 22, which we call Case II. In this case, $\mathcal{P} = 200$, $\mathcal{H}_c = 2000$, $\mathcal{C} = 0.05$, $\Theta_A = 0.5$, $G = 0.15$ and $M = -M_c = 0.01$. Here we could think of the spreading as taking place between the angles of 30 and 10 degrees; then $t = 1900$ is roughly one second. The solutal Marangoni effect dies off during the time the thermal Marangoni effect becomes important. If less spreading occurs, the time scales of the solutal and thermal Marangoni effects overlap for a wider range of parameters, which results in (in this case) "addition" of the two effects. While this particular run illustrates clearly the effects of fluid dynamics, it is relatively brief in terms of the duration of spread for typical solder spreading.

6. Discussion and Conclusion

The computational approach to the spreading of a drop was verified against previously known solutions in the presence of capillarity, gravity, and thermocapillarity (Marangoni effect) given by Ehrhard and Davis.[27] The good agreement of our results for the non-reactive cases indicates that the method works reasonably well for nonzero advancing equilibrium contact angles. When the advancing equilibrium contact angle is zero (perfect wetting case), we find that our numerical approach breaks down late in the spreading process when the Marangoni effect is present. Because the rate of change of the radius is slow by this time, we expect that the computed answer is a reasonable estimate of the final radius. As expected, the agreement between our computed solutions and the $\mathcal{C} = 0$ solutions improved with increasing time. The agreement improves for decreasing $\mathcal{C}$ as well.

An interesting feature from our computational results is the dependence of the *final radius* on the slip coefficient when the Marangoni effect is present. For the parameters we used, a slip coefficient less than about $\beta_1 = 10^{-4}$ was required to get a final radius that was insensitive to the value of the slip coefficient.

In contrast with the drops of uniform concentration, the results of the computations in the reactive case have no limiting analytical solution for comparison. The solute field generates complicated flow patterns early in the computation; it may generate a vortex within the flow field that would otherwise be dominated by capillarity when the solute field is absent. Depending on the extent of spreading, the model may allow for an intermediate period where capillarity dominates before thermal Marangoni effects take over. Thus the results also indicate that the solute diffuses out to the substrate relatively quickly compared to the spreading of the drop. The theory presented here with reactive effects corresponds to a fluid that has higher diffusivity than Pb-Sn solder, and this

is certainly a large part of the cause of the relatively fast behavior of the solute field. The higher diffusivity used in the results of this paper is apparent upon solving for the diffusivity given the Péclet number $\mathcal{P} = 200$. It is then clear we are operating in the range from about 10^{-3} to about $10^{-1}\mathrm{cm}^2/\mathrm{s}$ for the diffusivity, depending on the initial angle and radius given the estimate we use for κ. It may possible to build more complex behavior into the spatial shape of the solute field, and presumably to access more extreme diffusivities, but this comes at the cost of adding additional free parameters into the problem. The possibility remains that the our model may apply to situations other than metal/metal systems, e.g., organics.

We have proposed a model for reactive partial wetting situation that attempts to characterize spreading in many metal/metal systems. One of the central features in the model we propose is to incorporate a constitutive law for the contact line motion in order to treat a macroscopic fluid dynamics problem.[27] Use of the assumption of perfect wetting ($\theta_A = 0$) with this constitutive law leads to orders-of-magnitude discrepancy with experimental results as pointed out in Yost et al.[5] and Ambrose et al.[4] While the geometry of the model is planar, rather than axisymmetric, we find that the time scale to complete nearly all of the spreading is definitely of the correct order (about 1-10 seconds depending on the flux used for some unpublished spreading results for fluxed Pb-Sn on several different Cu and Cu-Sn-intermetallic substrates[42]). The same can be said for the time scales of previous theories of Boettinger et al.,[2] (although they did not point this out in their work) and of Ehrhard and Davis.[27]

Many issues remain to be addressed in this area. The contact angle may depend on many variables and parameters in the problem.[2] We have also neglected the effects of flux, which are important in terms of wettability, but may also be important in terms of the fluid dynamics during wetting. A more complete treatment of the large Péclet number transport would be desirable.

Acknowledgements

References

[1] W.J. Boettinger, C.A. Handwerker, and L.C. Smith, "On the wetting of the intermetallics Cu_6Sn_5 and Cu_3Sn by Pb-Sn alloys," in *The Science of Metal Joining*, edited by M.J. Cieslak, et al, (The Minerals, Metals and Materials Society, Warrendale, PA, 1992) pp. 183-189.

[2] W.J. Boettinger, C.A. Handwerker, and U.R. Kattner, "Reactive wetting and intermetallic formation," in *The Mechanics of Solder Alloy Wetting and Spreading*, edited by F. Yost et al., (The Minerals, Metals and Materials Society, Warrendale, PA, 1993).

[3] J.C. Ambrose, M.G. Nicholas, and A.M. Stoneham, "Dynamics of braze spreading," Acta metall. mater. **40**, 2483 (1992).

[4] J.C. Ambrose, M.G. Nicholas, and A.M. Stoneham, "Dynamics of liquid drop spreading in metal-metal systems," Acta metall. mater. **41**, 2395 (1993).

[5] F.G. Yost, F.M. Hosking, and D.R. Frear, "Introduction: The mechanics of solder alloy wetting and spreading" in *The Mechanics of Solder Alloy Wetting and Spreading*, edited by F. Yost *et al.*, (The Minerals, Metals and Materials Society, Warrendale, PA, 1993).

[6] A.E. Schwanke, W.L. Falke, and V.R. Miller, "Surface tension and density of liquid tin-lead solder alloys," J. Chem. Eng. Data **23**, 298 (1978).

[7] D.W.G. White, "The surface tensions of Pb, Sn, and Pb-Sn alloys," Met. Trans. **2**, 3067 (1971).

[8] H.R. Thresh and A.F. Crawley, "The viscosities of lead, tin and Pb-Sn alloys," Met. Trans. **1**, 1531 (1971).

[9] R.J. Klein-Wassink, *Soldering in Electronics*, Electrochemical Publishing Ltd., Ayr, Scotland, 1984).

[10] C. Huh and L.E. Scriven, "Hydrodynamic model of steady movement of a solid/liquid/fluid contact line," J. Coll. Int. Sci. **35**, 85 (1971).

[11] E.B. Dussan V. and S.H. Davis, "On the motion of a fluid-fluid interface along a solid surface," J. Fluid Mech. **65**, 71 (1974).

[12] E.B. Dussan V., "The moving contact line: the slip boundary condition," J. Fluid Mech. **77**, 665 (1976).

[13] L.M. Hocking, "A moving fluid interface. Part 2. The removal of the force singularity by a slip flow," J. Fluid Mech. **79**, 209 (1977).

[14] E.B. Dussan V. "On the spreading of liquids on solid surfaces: static and dynamic contact lines," Ann. Rev. Fluid Mech. **11**, 371 (1979).

[15] P.G. de Gennes, "Wetting: statics and dynamics," Rev. Mod. Phys. **57**, 827 (1985).

[16] D. Ausseré, A.M. Picard, and L. Legér, "Existence and Role of the Precursor Film in the Spreading of Polymer Liquids," Phys. Rev. Lett. **57**, 2671 (1986).

[17] L. Legér, M. Erman, A.M. Guinet-Picard, D. Ausseré, and C. Strazielle, "Precursor Film Profiles of Spreading Liquid Drops," Phys. Rev. Lett. **60**, 2360 (1988).

[18] H.P. Greenspan, "On the motion of a small viscous droplet that wets a surface," J. Fluid Mech. **84**, 125 (1978).

[19] H.P. Greenspan and B.M. McCay, "On the wetting of a surface by a very viscous fluid," Stud. Appl. Math. **69**, 95 (1981).

[20] L.M. Hocking, "Sliding and spreading of thin two-dimensional drops," Quart. J. Mech. appl. Math. **34**, 37 (1981).

[21] L.M. Hocking and A.D. Rivers, "The spreading of a drop by capillary action," J. Fluid Mech. **121**, 425 (1982).

[22] L.M. Hocking, "The spreading of a thin drop by gravity and capillarity," Quart. J. Mech. appl. Math. **36**, 55 (1983).

[23] L.M. Hocking, "Rival contact-angle models and the spreading of drops," J. Fluid Mech. **239**, 671 (1991).

[24] L. Tanner, "The spreading of silicone oil drops on horizontal surfaces," J. Phys. D **12**, 1473 (1979).

[25] P.G. de Gennes, X. Hua, and P. Levinson, "Dynamics of wetting: local contact angles," J. Fluid Mech. **212**, 55 (1990).

[26] F. Brochard-Wyart, H. Hervet, C. Redon, and F. Rondelez, "Spreading of 'Heavy' Droplets I. Theory," J. Coll. Int. Sci. **142**, 518 (1991).

[27] P. Ehrhard and S.H. Davis, "Non-isothermal spreading of liquid drops on horizontal plates," J. Fluid Mech. **229**, 365 (1991).

[28] P. Ehrhard,"Experiments on isothermal and non-isothermal spreading," J. Fluid Mech. **257**, 463 (1993).

[29] M.K. Smith, "Thermocapillary migration of a two-dimensional liquid droplet on a solid surface," (1993), pending publication.

[30] D.M. Anderson and S.H. Davis, "The spreading of volatile liquid droplets on heated surfaces," Phys. Fluids (to appear).

[31] M.L. Ford and A. Nadim, "Thermocapillary migration of an attached drop on a solid substrate," (1994), pending publication.

[32] H. Schlichting, Boundary-Layer Theory, (McGraw-Hill, New York, 1979).

[33] B. Reisfeld, S.G. Bankoff, and S.H. Davis, "The dynamics and stability of thin liquid films during spin coating. I. Films with constant rates of evaporation or absorption," J. Appl. Phys. **70**, 5258 (1991).

[34] B. Reisfeld, S.G. Bankoff, and S.H. Davis, "The dynamics and stability of thin liquid films during spin coating. II. Films with unit order and large Peclet numbers," J. Appl. Phys. **70**, 5267 (1991).

[35] P.J. Haley and M.J. Miksis, "The effect of the contact line on droplet spreading," J. Fluid Mech. **229**, 365 (1991).

[36] B.T. Murray, R.J. Braun, W.J. Boettinger and G.B. McFadden, in preparation.

[37] C. Redon, F. Brochard-Wyart, H. Hervet, and F. Rondelez, "Spreading of 'Heavy' Droplets II. Experiments," J. Coll. Int. Sci. **149**, 580 (1992).

[38] C. Canuto, M.Y. Hussaini, A. Quarteroni, T.A. Zang, *Spectral methods in fluid dynamics*, (Springer-Verlag, Berlin, 1988).

[39] L.R. Petzold, "A description of DASSL: A differential/algebraic system solver," (Sandia National Laboratories, Albuquerque, NM, 1982), SAND82-8637.

[40] D.M. Anderson and S.H. Davis, "Two-fluid viscous flow in a corner," J. Fluid Mech. **257**, 1 (1993).

[41] D.M. Anderson and S.H. Davis, "Local fluid and heat flow near contact lines," J. Fluid Mech. **268**, 231 (1994).

[42] W.J. Boettinger, and C.A. Handwerker, unpublished NIST research.

Density	ρ	8.3 gm/cm^3
Viscosity	μ	1.8×10^{-2} g/(cm s)
Diffusion coefficient	D	2.7×10^{-5} cm^2/s
Surface tension	σ_w	500 erg/cm^2
Thermal Marangoni effect	γ_T	0.05 erg/(cm^2 K)
Solutal Marangoni effect	γ_c	-1.0 erg/(cm^2 wt %)
Thermal conductivity	λ	5.0×10^6 erg/(cm K S)
Heat capacity	c_p	2.2 ×10^6 erg/(gm k)
Temperature difference	ΔT	100 K
Concentration difference	Δc	1.0 wt %
Contact line mobility	κ	1.35 ×10^3 cm/s

Table 1: The material parameters are for Pb-Sn. The parameters for the passive gas (air) above are assumed to be such that the Biot number is fixed at $B = 0.1$. The contact line mobility and the temperature and concentration differences are estimates.

G	Asymptotic	Numerical
0.001	1.732224	1.732224
0.01	1.733783	1.733784
0.1	1.749371	1.749481
1.0	1.905256	1.915288

Table 2: A comparison of our numerical results with the asymptotic results of Ehrhard and Davis[27] for the final radius a_∞ of an isothermal drop with gravity. Here $\Theta_A = 1/2$, and so $a_\infty^0 \equiv \sqrt{3/(2\Theta_A)} = \sqrt{3}$. Their asymptotic results are given by $a_\infty = a_\infty^0[1 + (a_\infty^0)^2 G/30]$.
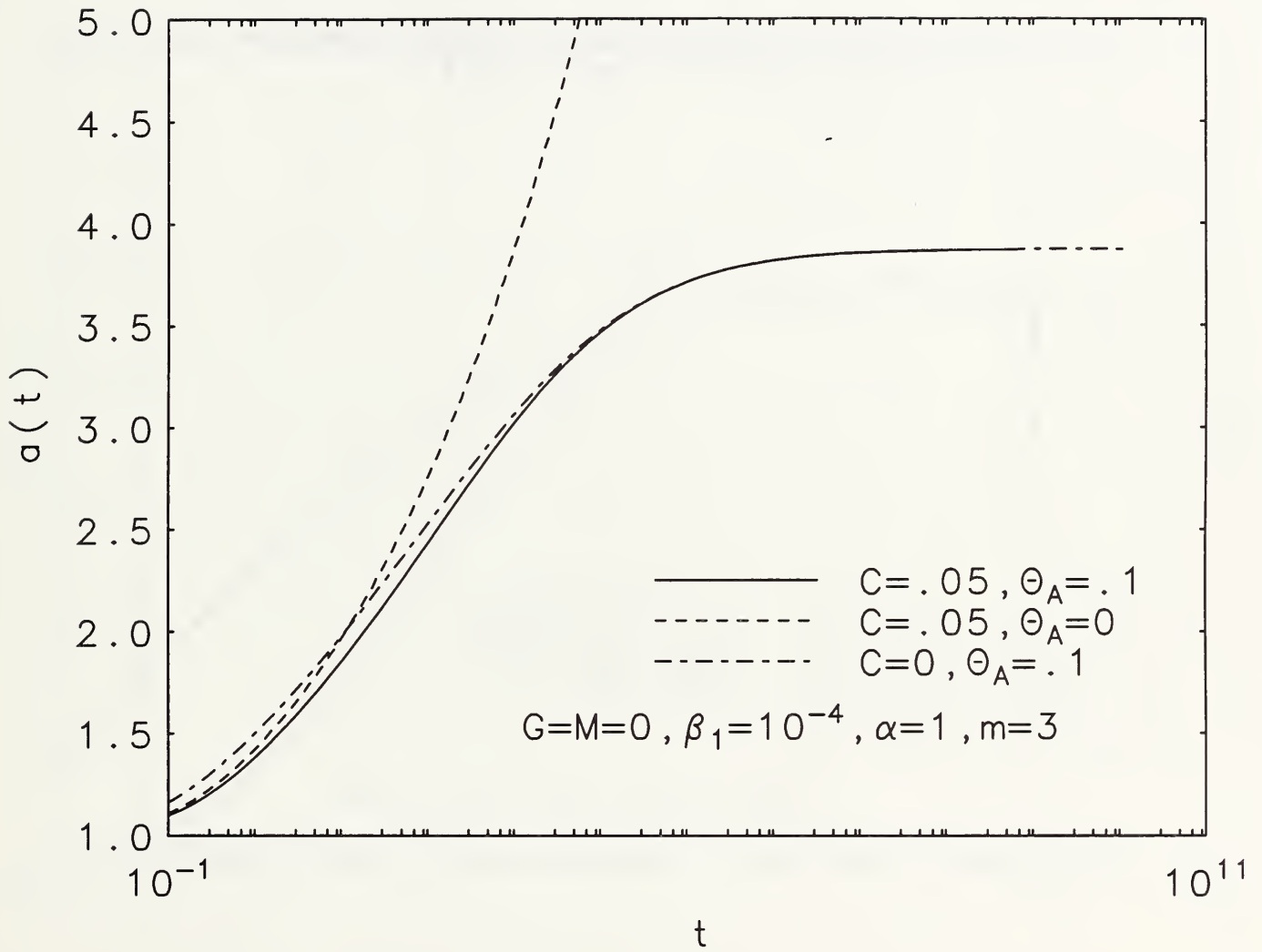
Figure 1: Radius $a(t)$ for pure capillary spreading. The $C = 0$ case is for the spreading of a circular cap.
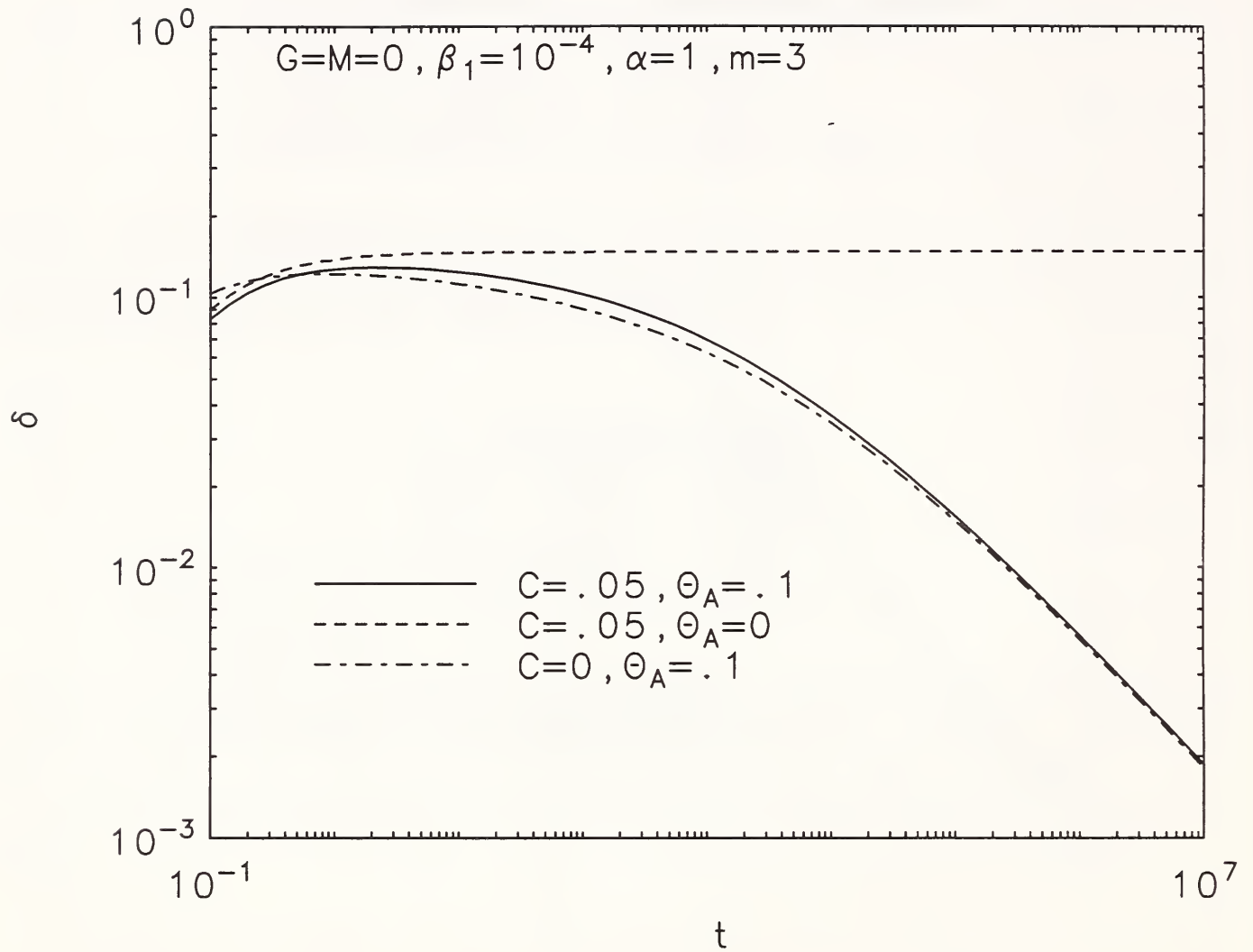
Figure 2: Spreading exponent δ for pure capillary spreading. The $C = 0$ case is for the spreading of a circular cap.
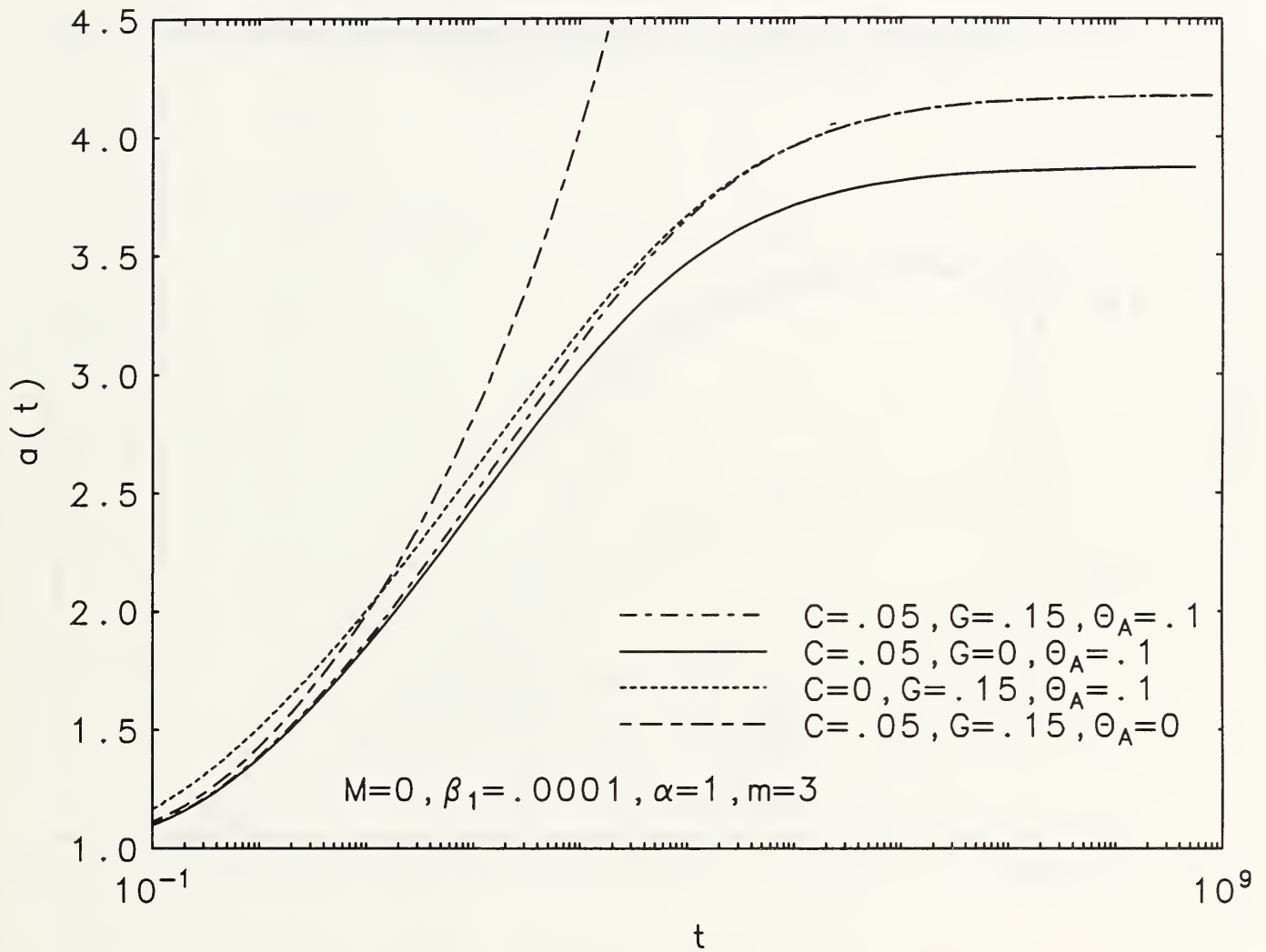
Figure 3: Radius $a(t)$ for spreading with capillarity and gravity. The $\mathcal{C} = 0$ case is for quasistatic spreading of a cap with gravity.
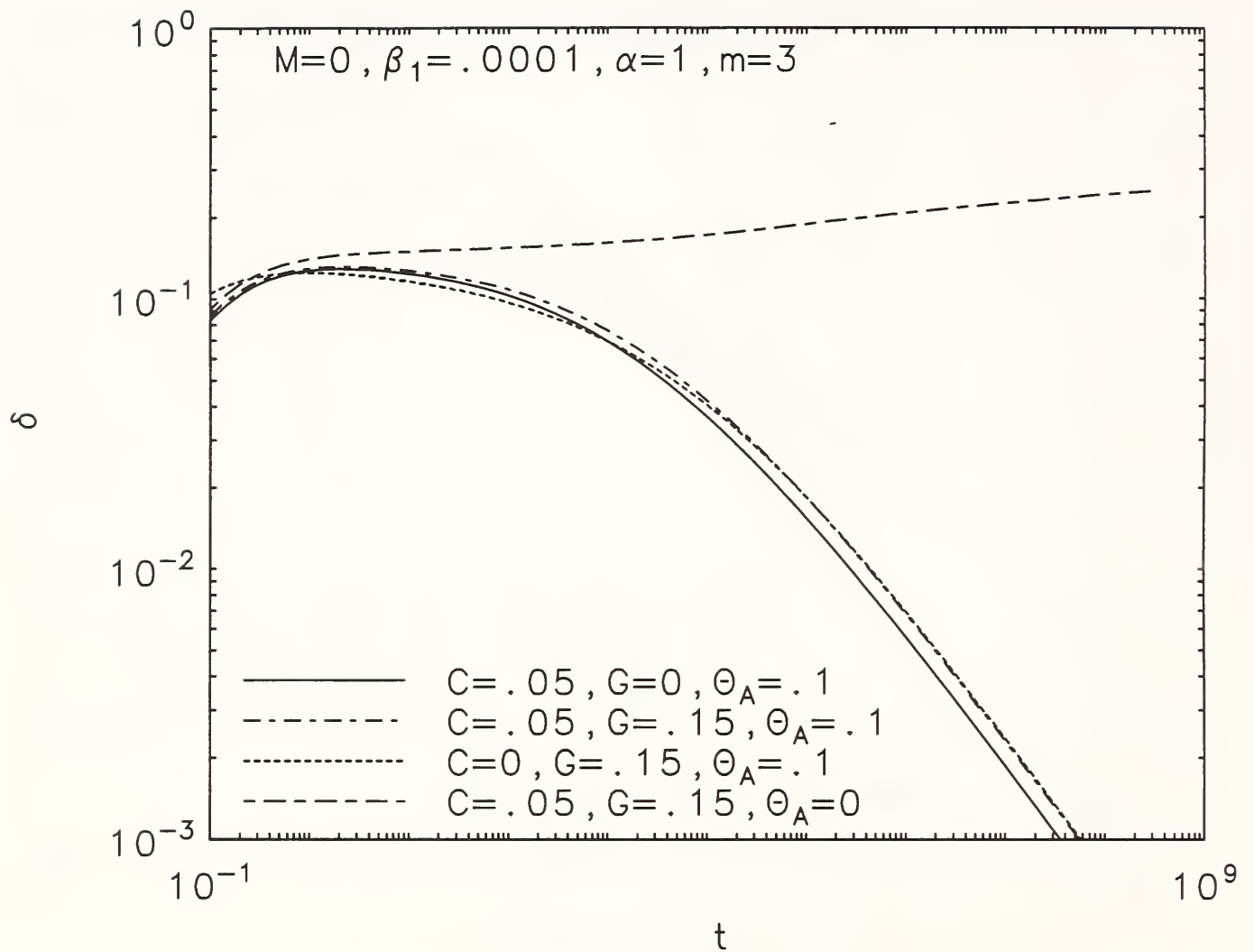
Figure 4: Spreading exponent δ for $M = 0$. The $C = 0$ case is for quasistatic spreading of a cap with gravity. The spreading exponent asymptotes to $\delta = 0.25$ for the perfectly wetting case.
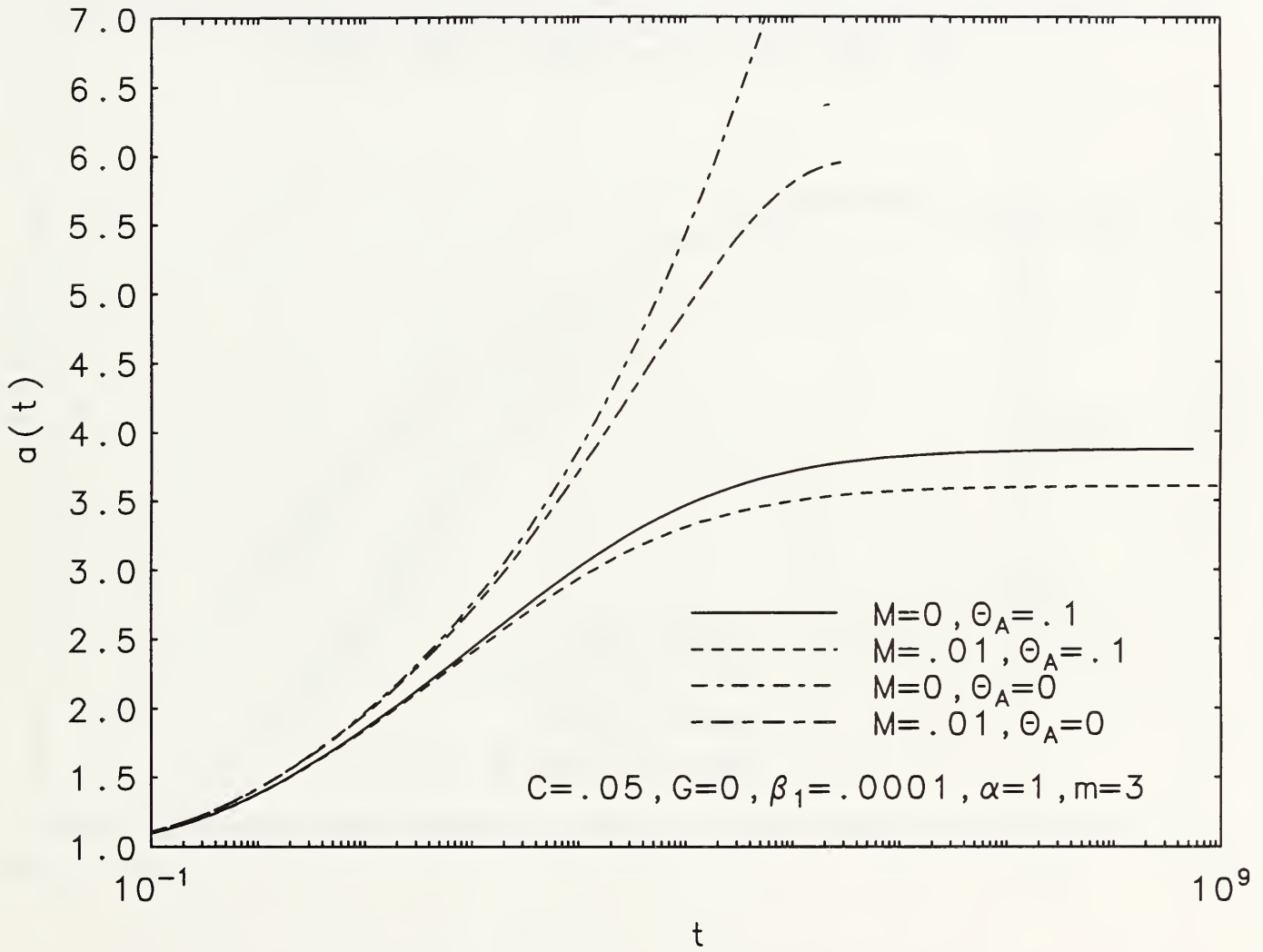
Figure 5: Radius $a(t)$ for spreading with thermocapillarity.
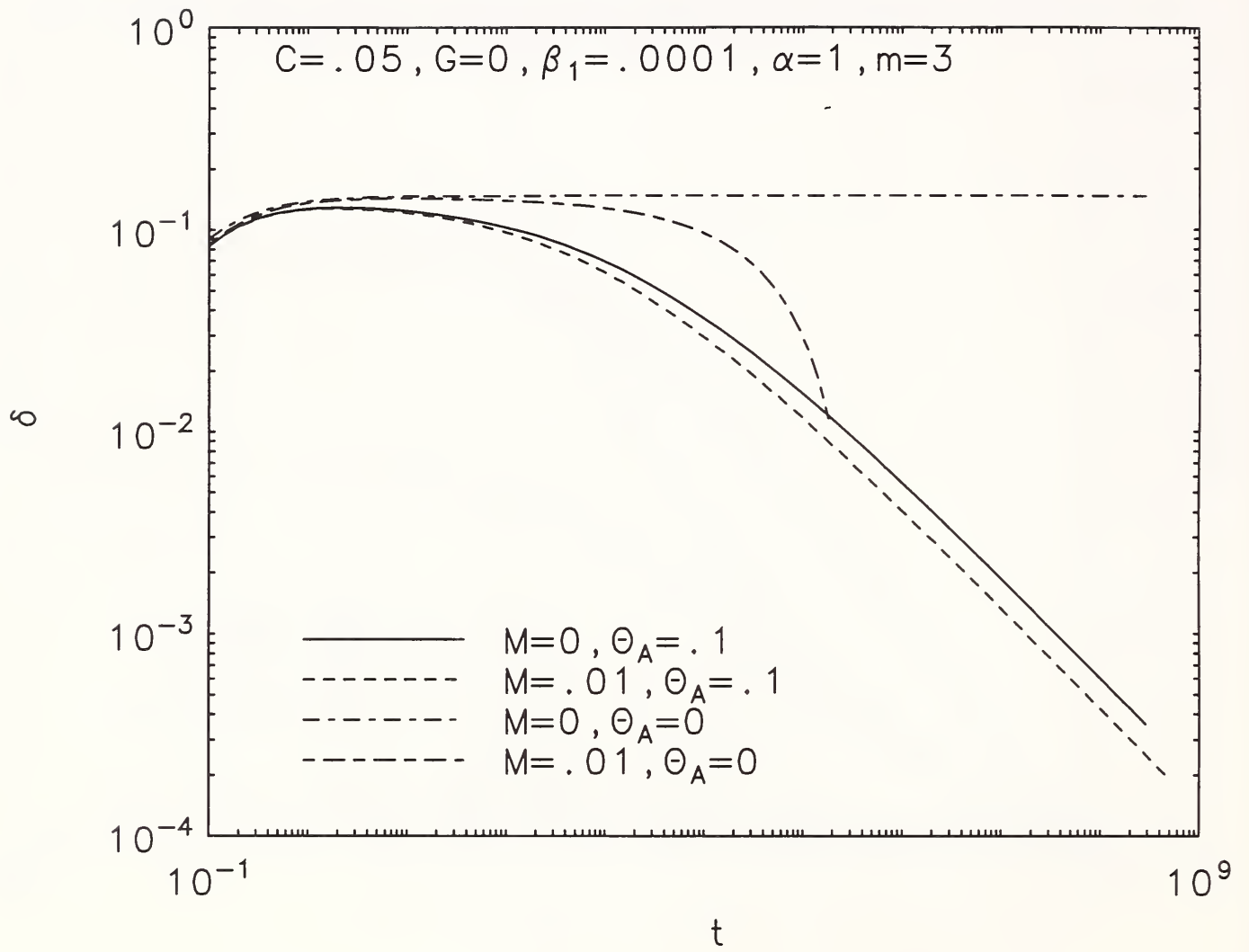
Figure 6: Spreading exponent δ for capillary spreading with thermocapillarity.
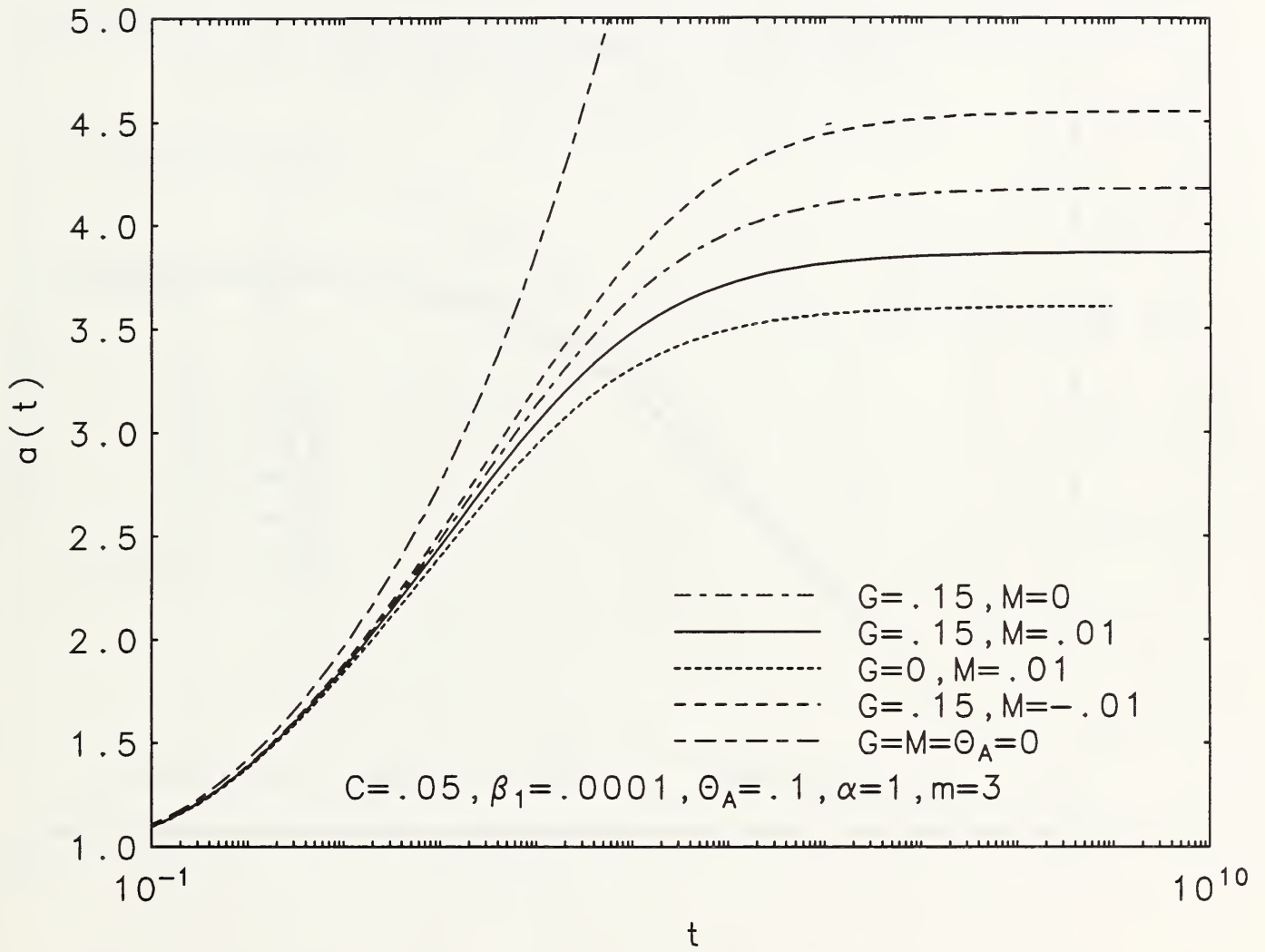
Figure 7: Radius $a(t)$ for capillary spreading with gravity and thermocapillarity. For $M = 0.01$, the Marangoni effect retards spreading; the case with the opposite sign promotes spreading.
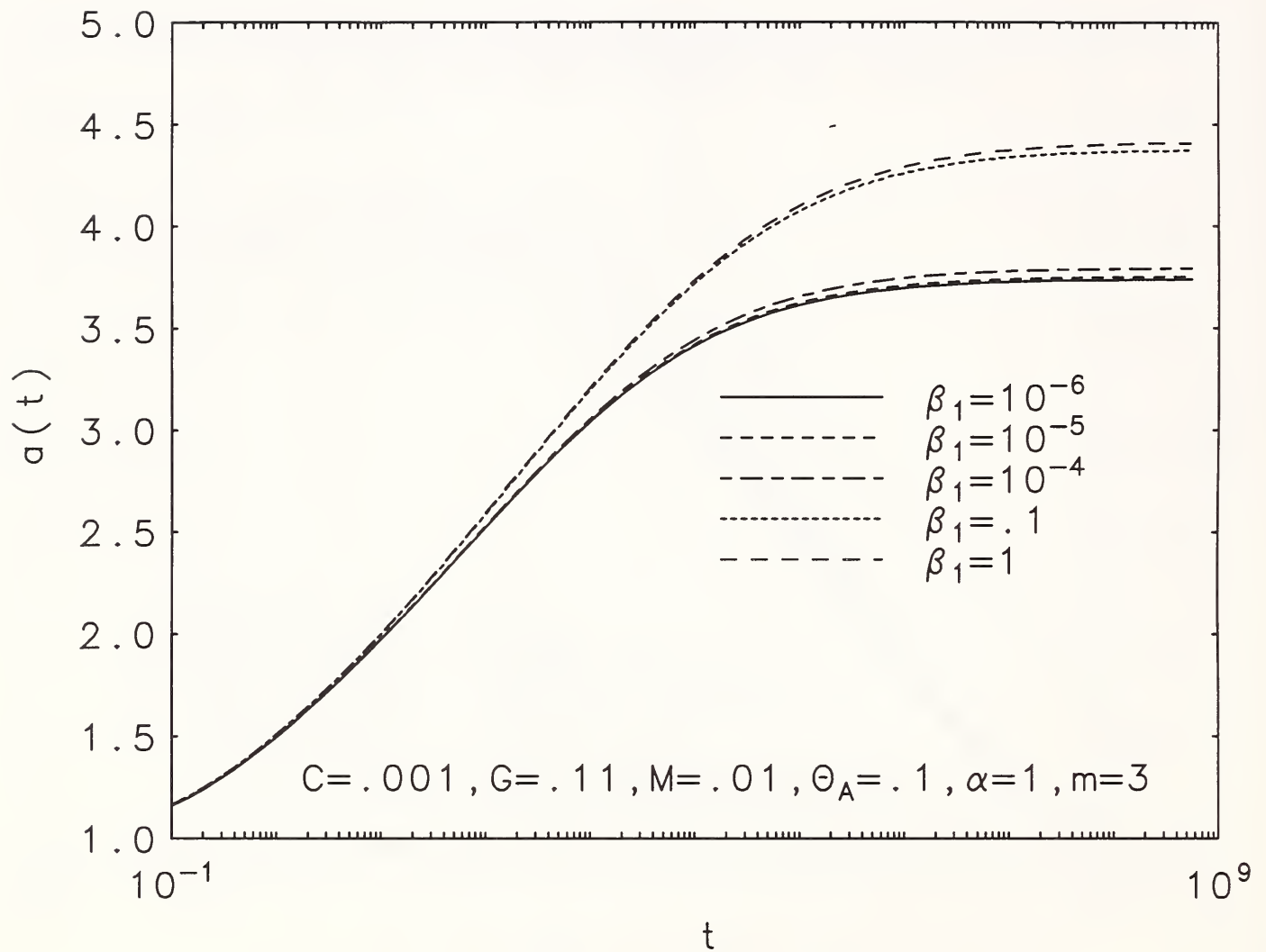
Figure 8: Radius $a(t)$ for capillary spreading with gravity and thermocapillarity as a function of β_1. The small capillary number solutions now depend on the slip coefficient.
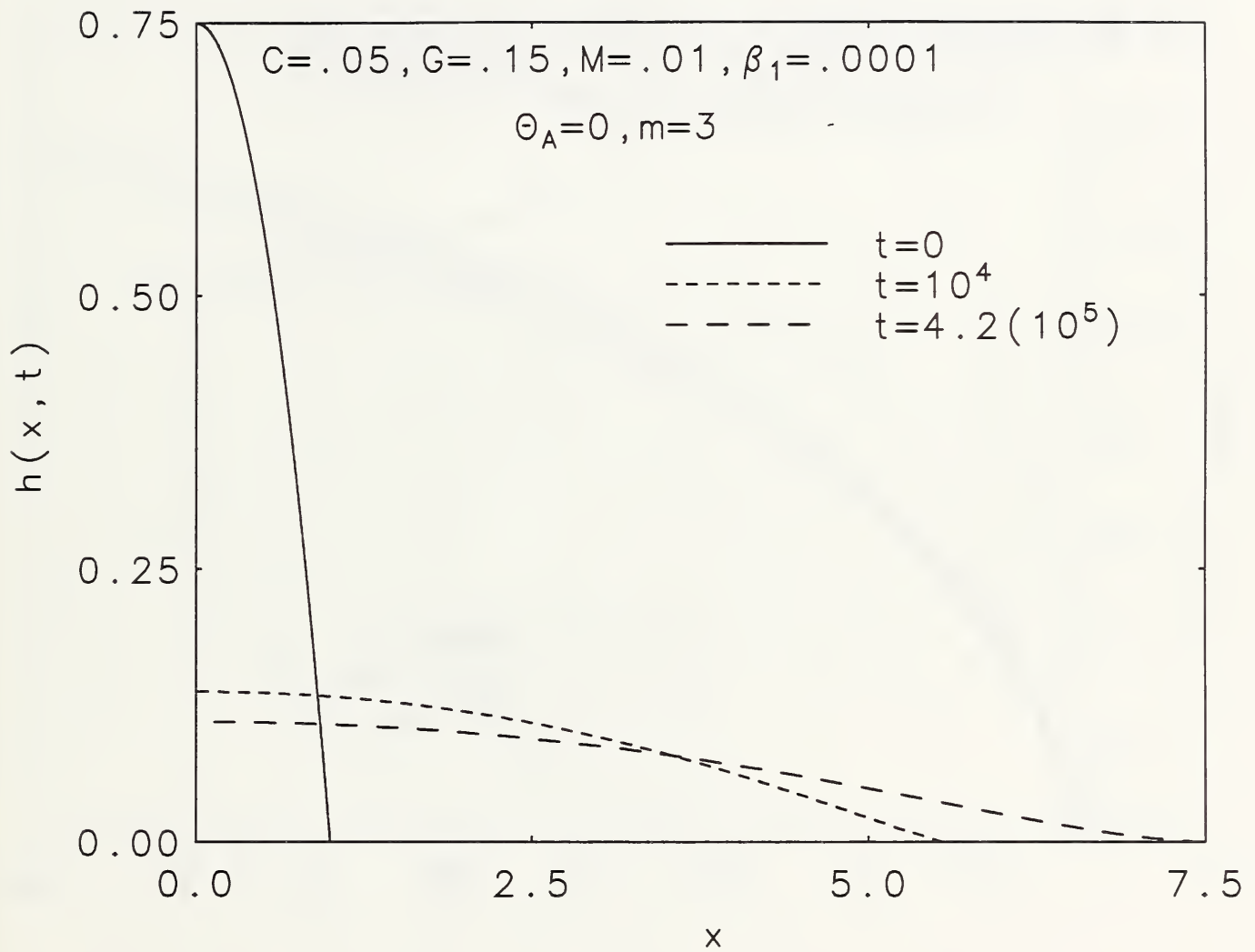
Figure 9: Droplet shapes for various times for capillary spreading with gravity and thermocapillarity.
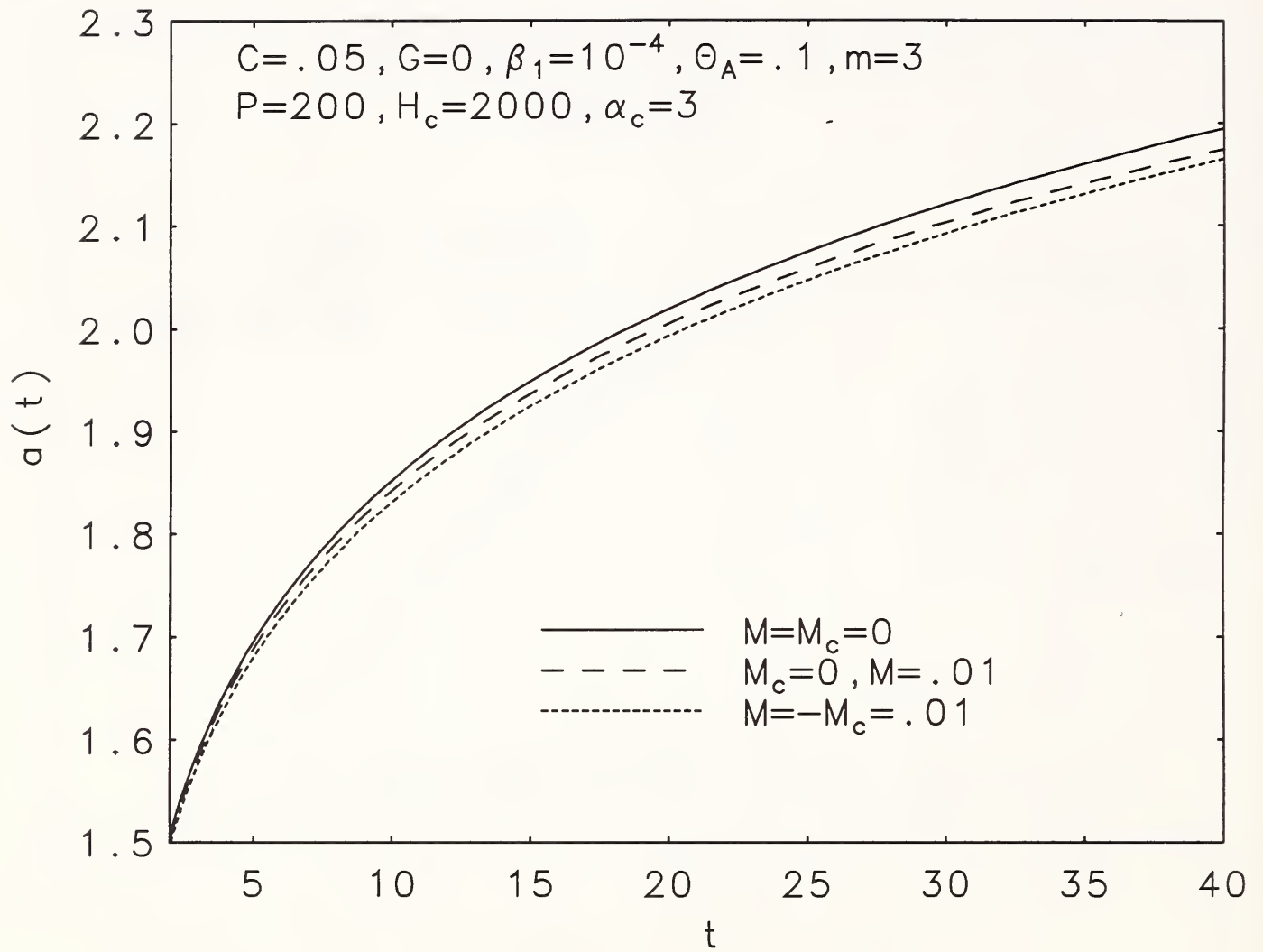
Figure 10: Drop radius as a function of time. Only thermo- and soluto-capillary effects are included here. At longer times, the two curves involving the Marangoni effects merge.
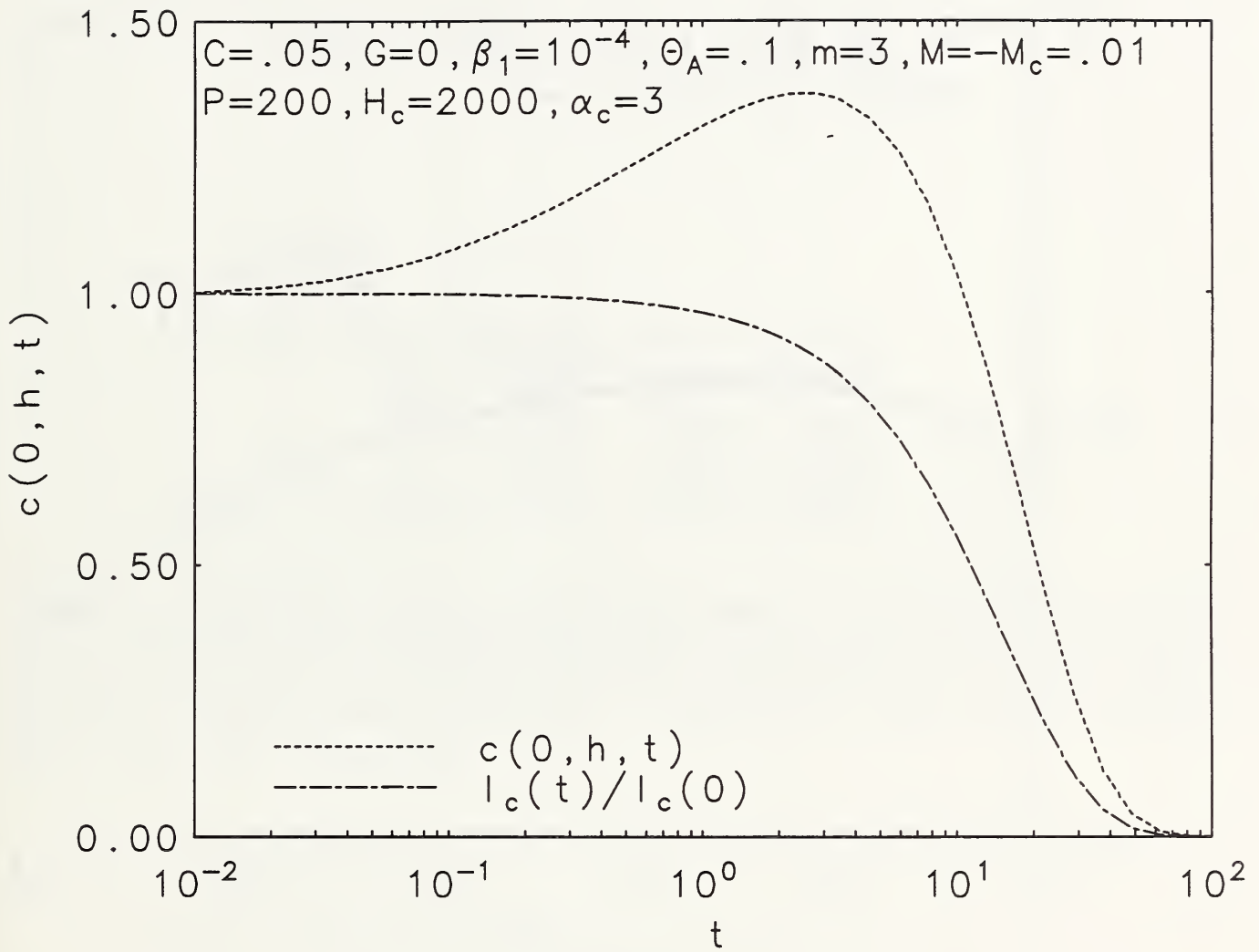
Figure 11: Concentration at the top of the drop as a function of time, and the total amount of solute $I_c(t)$ normalized by its initial value $I_c(0)$. Only thermo- and soluto-capillary effects are included here.
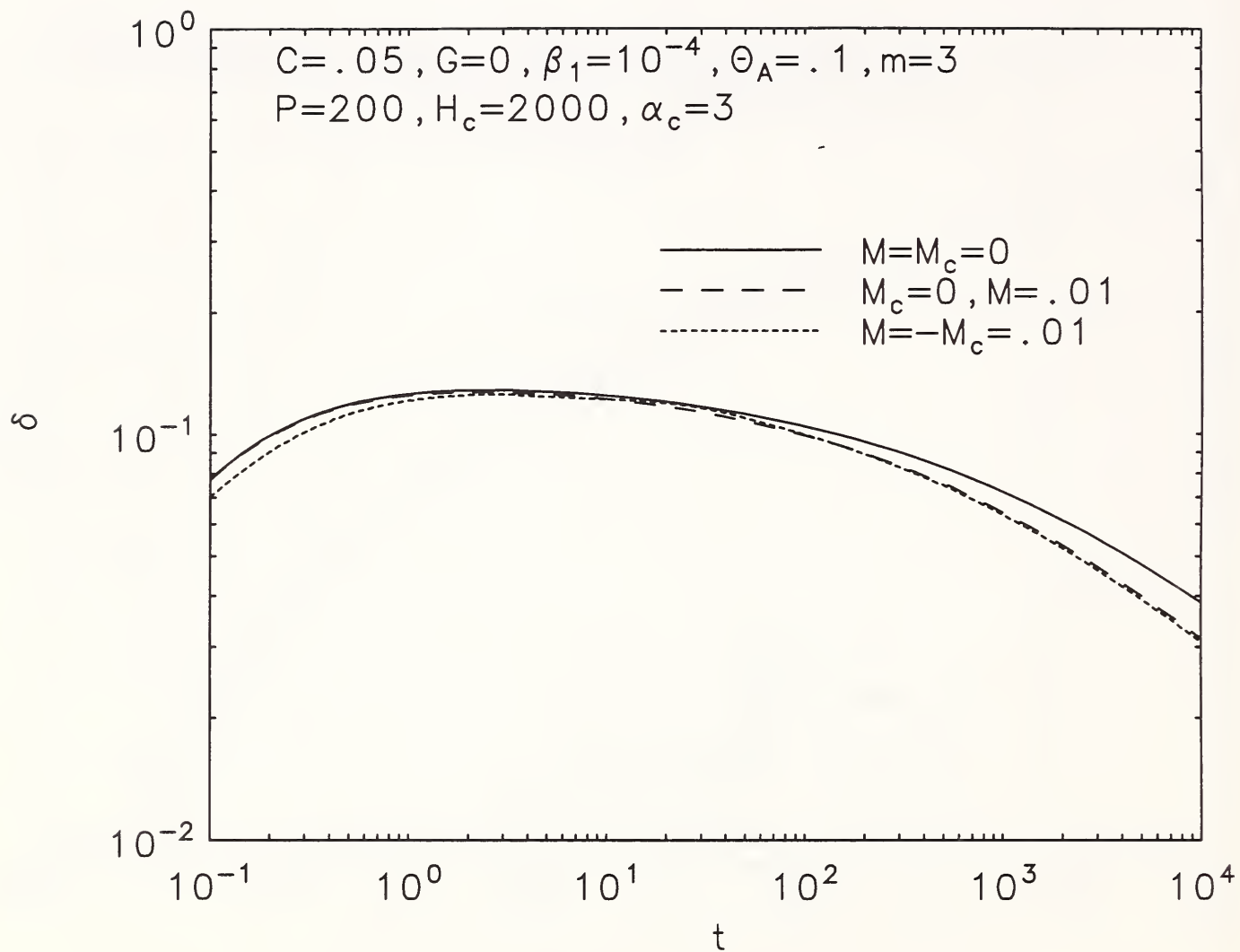
Figure 12: Exponent of drop radius as a function of time. Only thermo- and soluto-capillary effects are included here. The slowing of the growth of the radius at early times can be seen by a lowered δ, but at later times the radius catches up to the case of the pure drop with $M = 0.01$.

M	Asymptotic	$B = 0$	$B = 0.1$
0.001	1.73055	1.73067	1.72943
0.01	1.71705	1.71859	1.71907
0.1	1.58205	1.61122	1.61539
0.25	1.35705	1.47430	1.48254

Table 3: A comparison of our numerical results with the asymptotic results of Ehrhard and Davis[27] for the final radius a_∞ of an nonisothermal drop without gravity. The columns $B = 0$ denotes the case when $M \neq 0$, but $B = 0$ in the denominator of the Marangoni term in the evolution equation (for direct comparison with Ref. 27). Here $\Theta_A = 1/2$, and $a_\infty^0 = \sqrt{3}$. Their asymptotic results are given by $a_\infty = a_\infty^0[1 + M a_\infty^0/(4\Theta_A)]$.
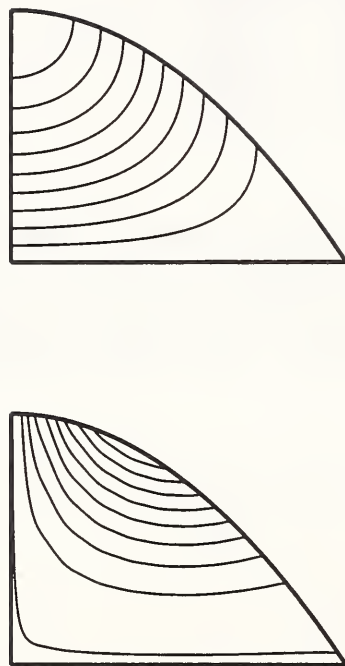
Figure 13: Case I, $t = 0$. The top figure is the initial dimensionless concentration field c (in steps of $\Delta c = 0.1$) and the bottom is the initial stream function ψ (in steps of $\Delta \psi = 0.01$). The concentration and stream function are both zero at the substrate for this and all subsequent figures. The stream function indicates the dominance of capillary spreading initially.
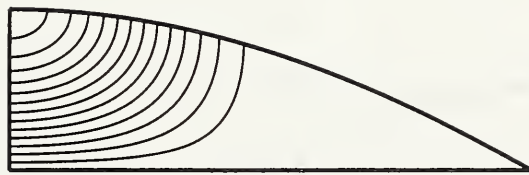
Figure 14: Case I, $t = 3.0$, $\Delta c = 0.1$, and $\Delta \psi = 0.001$. The stream function is already being strongly affected by the solute gradient on the free surface, and the concentration at the top, center of the drop has increased due to the flow sweeping the alloying element there.
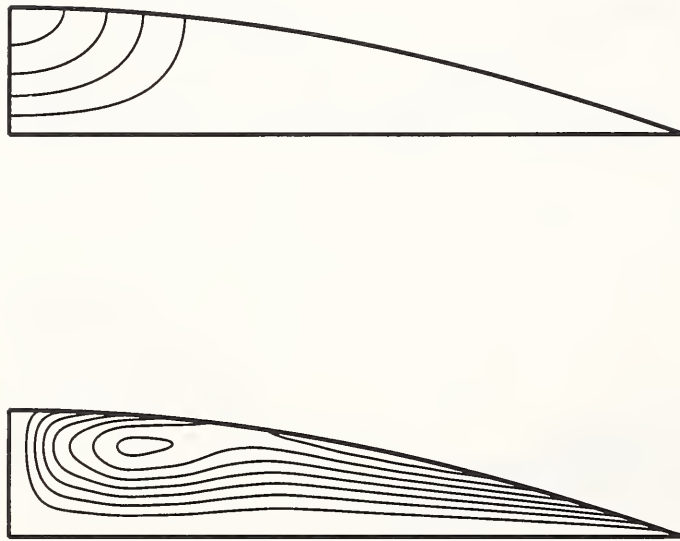
Figure 15: Case I, $t = 22.0$, $\Delta c = 0.1$, and $\Delta\psi = 0.0002$. A vortex has formed as a result of the solute gradient. Note the rapid decrease of the maxima of the stream function and the solute profile.
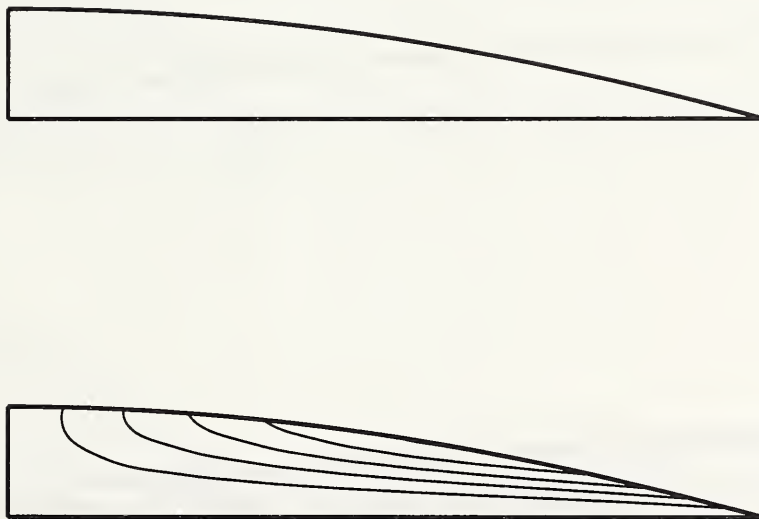
Figure 16: Case I, $t = 62.9$ and $\Delta\psi = 0.0001$. The stream function is no longer affected by the concentration since the maximum concentration is now well below 1% of the initial value; we no longer show the concentration field because of this. Note the continued decrease in the maximum of the stream function. The stream lines do not indicate strong effects from thermocapillarity yet.
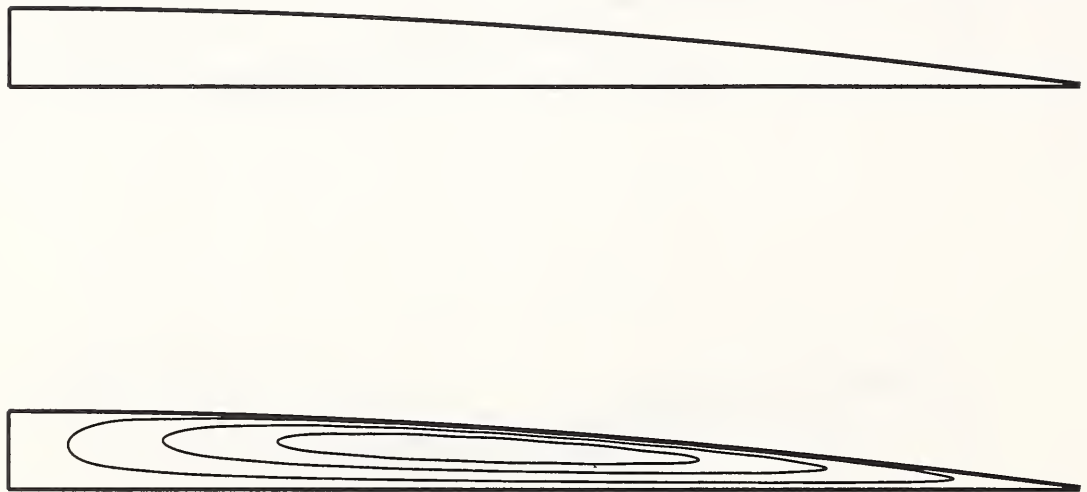
Figure 17: Case I, $t = 7071.$, and $\Delta\psi = 0.000005$. The maximum concentration field has decreased to far below 1% of its original maximum, and so we no longer display its contours. A single vortex which is rather weak in magnitude occupies the drop. The spreading of the drop is about 86% complete.
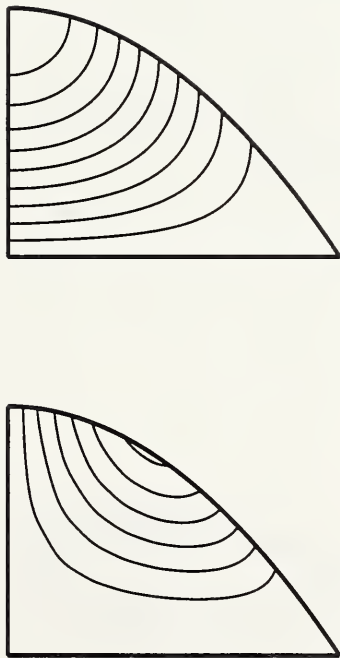
Figure 18: Case II, $t = 0$. The top figure is the initial dimensionless concentration field c (in steps of $\Delta c = 0.1$) and the bottom is the initial stream function ψ (in steps of $\Delta \psi = 0.01$) for case II. The stream function indicates the dominance of capillary spreading initially; the streamlines have been turned somewhat by the presence of gravity.
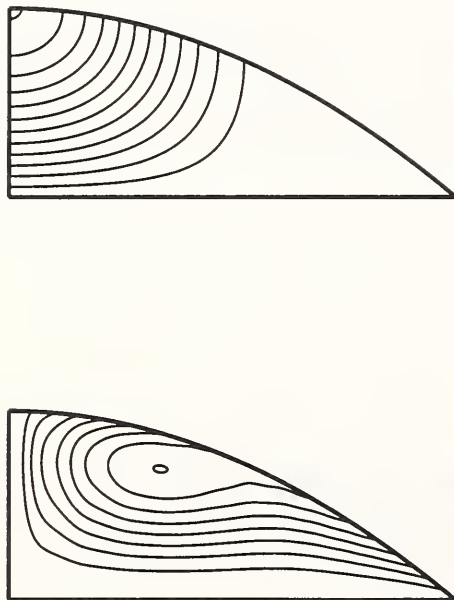
Figure 19: Case II, $t = 3.0$, $\Delta c = 0.1$, and $\Delta \psi = 0.001$. The stream function is already being strongly affected by the solute gradient on the free surface, and the concentration at the top of the drop has increased due to the flow sweeping the alloying element there.
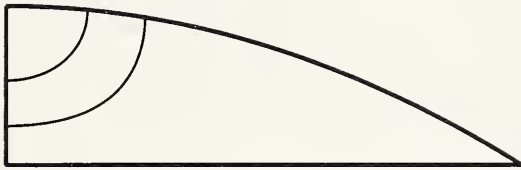
Figure 20: Case II, $t = 22.0$, $\Delta c = 0.1$, and $\Delta \psi = 0.0002$. A vortex has formed as a result of the solute gradient. Note the rapid decrease of the maxima of the stream function and the solute profile.
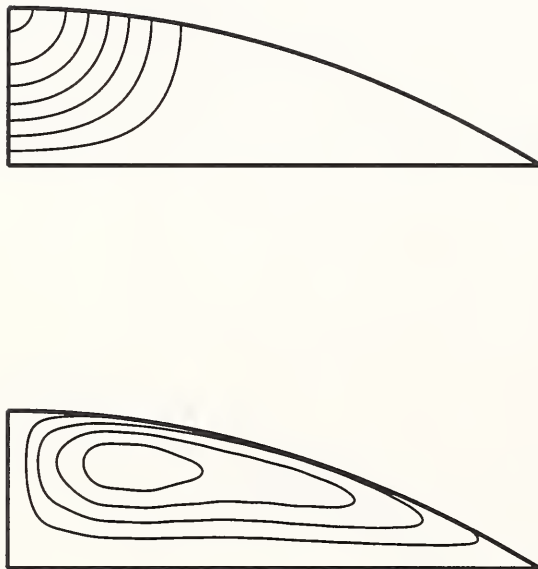
Figure 21: Case II, $t = 62.9$, $\Delta c = 0.01$, and $\Delta \psi = 0.0001$. Note the smaller step size between concentration contours and the continued decrease in the maximum of the stream function. The stream lines do not indicate strong effects from thermocapillarity yet.
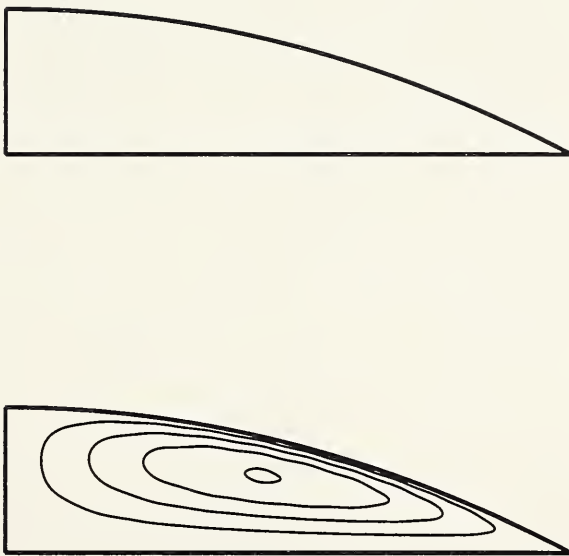
Figure 22: Case II, $t = 1465.$, and $\Delta\psi = 0.00005$. The maximum concentration field has decreased to far below 1% of its original maximum, and so we no longer display its contours. A single weak vortex occupies the drop. The spreading of the drop is about 98% complete.